

Article

Application of Least-Squares Support-Vector Machine Based on Hysteresis Operators and Particle Swarm Optimization for Modeling and Control of Hysteresis in Piezoelectric Actuators

Ayad G. Baziyad ^{*}, Adnan S. Nouh, Irfan Ahmad and Abdulaziz Alkuhayli 

Department of Electrical Engineering, College of Engineering, King Saud University, Riyadh 11421, Saudi Arabia; asnouh@ksu.edu.sa (A.S.N.); irfahmad@ksu.edu.sa (I.A.); aalkuhayli@ksu.edu.sa (A.A.)

* Correspondence: ayadgaafar@gmail.com

Abstract: Nanopositioning systems driven by piezoelectric actuators are widely used in different fields. However, the hysteresis phenomenon is a major factor in reducing the positioning accuracy of piezoelectric actuators. This effect makes the task of accurate modeling and position control of piezoelectric actuators challenging. In this paper, the learning and generalization capabilities of the model are efficiently enhanced to describe and compensate for the rate-independent and rate-dependent hysteresis using a kernel-based learning method. The proposed model is inspired by the classical Preisach hysteresis model, in which a set of hysteresis operators is used to address the problem of mapping, and then least-squares support-vector machines (LSSVM) combined with a particle swarm optimization (PSO) algorithm are used for identification. Two control schemes are proposed for hysteresis compensation, and their performance is evaluated through real-time experiments on a nanopositioning platform. First, an inverse model-based feedforward controller is designed based on the LSSVM model, and then a combined feedback/feedforward control scheme is designed using a classical control strategy (PID) to further enhance the tracking performance. For performance evaluation, different datasets with a variety of hysteresis loops are used during the simulation and experimental procedures. The results show that the proposed method is successful in enhancing the generalization capabilities of LSSVM training and achieving the best tracking performance based on the combination of feedforward control and PID feedback control. The proposed control scheme outperformed the inverse Preisach model-based control scheme in terms of both positioning accuracy and execution time. The control scheme that uses the LSSVM based on nonlinear autoregressive exogenous (NARX) models has significantly less computational complexity compared to our control scheme but at the expense of accuracy.

Keywords: piezoelectric actuators; least-squares support-vector machine (LSSVM); hysteresis; control



Citation: Baziyad, A.G.; Nouh, A.S.; Ahmad, I.; Alkuhayli, A. Application of Least-Squares Support-Vector Machine Based on Hysteresis Operators and Particle Swarm Optimization for Modeling and Control of Hysteresis in Piezoelectric Actuators. *Actuators* **2022**, *11*, 217. <https://doi.org/10.3390/act11080217>

Academic Editor: Katsushi Furutani

Received: 3 July 2022

Accepted: 28 July 2022

Published: 2 August 2022

Publisher's Note: MDPI stays neutral with regard to jurisdictional claims in published maps and institutional affiliations.



Copyright: © 2022 by the authors. Licensee MDPI, Basel, Switzerland. This article is an open access article distributed under the terms and conditions of the Creative Commons Attribution (CC BY) license (<https://creativecommons.org/licenses/by/4.0/>).

1. Introduction

Hysteresis effects have played a critical role in many nanopositioning systems that use piezoelectric actuators, such as microscopy [1] and nano-fabrication systems [2]. It means that output displacement of the actuator lags behind input voltage; this property can be seen as a form of a hysteresis loop [3]. Hence, hysteresis is considered as a multiple-valued mapping. Hysteresis characteristics have always had a significant impact on the resolution of nanopositioning systems [4]. In the literature, the hysteresis modeling and compensation methods of piezoelectric actuators are of great interest in improving their positioning accuracy. The improvement in the model fit can be obtained by accomplishing two tasks: the first is to introduce a suitable mapping of hysteresis so that multivalued mapping is transformed into a single-valued one; the second is to provide a model that can be effectively used to characterize both rate-independent and rate-dependent hysteresis [5]. The rate-independent hysteresis term indicates that the output displacement depends only on input voltage, while the rate-dependent hysteresis means that the output displacement

depends not only on input voltage but also on input frequency (or input rate) [6,7]. Traditional hysteresis models often fail to describe the rate-dependent behavior, such as the Duhem model [8,9], Bouc–Wen model [10], backlash model [6], Preisach model [9,11], Krasnoselskii–Pokrovskii (KP) model [12], and Prandtl–Ishlinskii (PI) model [13]. Some of these models have been improved to include rate-dependent hysteresis behavior, such as the generalized P-I model [14], and the improved Preisach model [15,16]. However, their implementation is usually very complicated [5,17,18] and they have a lot of parameters to be tuned. Hence, building hysteresis compensators based on the inverse of such models results in high implementation complexity.

To address the computational complexity issues, various types of machine learning techniques have been proposed in the literature, among them artificial neural networks (ANNs), which provide an effective approach to describing the complicated hysteresis non-linearity and can implement a nonlinear input–output mapping. For instance, the authors in [19] have proposed Multilayer Feedforward Neural Networks (MLFFNNs) for magnetic hysteresis modeling. They have used it successfully to represent the approximation of the Preisach distribution function. The simulation results have shown that artificial neural networks (ANNs) provide an efficient way to represent hysteresis. The authors in [20] have proposed a gray box neural network to identify the parameters of the rate-dependent hysteresis model for a piezoelectric actuated stage. The simulation results have been closer to the experimental data than the MLFFNNs. The authors in [21] have presented a deep learning method to further improve the control accuracy of the ANN. They have designed a feedforward controller based on a model of a recurrent neural network. The output displacement error has been reduced and the PEA-RNN outperformed the ANN with fewer training samples. However, the ANN-based models are prone to overfitting problems, as they may fall into the local minimum during the optimization procedure, which results in a low level of generalization, thus affecting the accuracy of the model [22,23].

To overcome the problem of overfitting, the support-vector machines (SVMs) [24] have been put forward. SVMs have higher generalization capabilities than the model based on the ANNs because they are based on the structural risk minimization (SRM) principle which reduces the upper bound of the generalization error, whereas ANNs are based on the principle of empirical risk minimization (ERM) which minimizes the error on the training data [25,26]. Least-squares support-vector machine (LSSVM) [27] is a modified version of the traditional SVM which utilizes equality constraints instead of inequality constraints and a squared loss function instead of the ϵ -insensitive loss function. This modification simplifies the problem and solves linear equations instead of quadratic programming used in SVM, thus making it better than SVM in terms of accuracy and computation time [27]. LSSVM techniques can only identify single-to-single mapping, whereas hysteresis exhibits multi-valued mapping. For this purpose, in literature, nonlinear autoregressive exogenous (NARX) models have been employed [28–30]. This method is based on expanding input space into multidimensional space, where the current output depends on the current input and previous inputs and outputs. The feedforward control based on the inverse hysteresis model requires that the LSSVM-NARX model is pre-trained to learn their inverse dynamics and then used as a direct controller. The authors in [31] have developed a feedforward controller and employed the measured displacement as a feedback correction so that the past displacement input includes the desired displacement and the measured displacement according to a certain ratio. Although LSSVM-NARX models have been employed successfully, more research is needed to address the problem of error accumulation owing to the feedback of the inverse model [32].

The author in [33] has proposed a model to describe the rate-independent and rate-dependent hysteresis based on a kernel-based learning method. This model is inspired by the classical Preisach hysteresis model in which a set of stop operators is used to address the problem of mapping and then least-squares support-vector machines (LSSVMs) are used for identification. One of the main advantages of this model is that it is not susceptible to error accumulation as there is no feedback from the output of the model back to the input.

Meanwhile, it is easy to obtain enough representative training data through small numbers of hysteresis operators. The datasets for the hysteresis loops have been generated using the Prandtl–Ishlinskii model [34] for magnetostrictive actuators. The obtained datasets have been then used to train and validate the proposed hysteresis model as well as to evaluate the control strategy performance. The simulation results have shown that LSSVM provides higher accuracy and better tracking performance compared to ANN and NARX-based models. This method has been only tested for modeling and controlling a specific type of actuator. Additionally, machine learning applications usually require an intelligent optimization algorithm to fine-tune the hyper-parameters [35,36], while the author has used Coupled Simulated Annealing (CSA) and simplex method to optimize the hyper-parameters of LSSVM; this strategy has a probability to accept a worse solution than the current solution, and thus it does not guarantee finding of a global optimum. Moreover, the practical issues of control have not been investigated in his study.

In this study, LSSVM based on a stop operator for mapping problems is evaluated for modeling and controlling a piezoelectric actuator in a nanopositioning system. The main contribution of this study is to evaluate a control strategy for piezoelectric actuators, based on LSSVM as an intelligent tool to provide more accurate position tracking than LSSVM-NARX models and has less execution time than that based on Preisach. For this purpose, a multiple-valued mapping is first converted into a one-to-one mapping using a strategy inspired by the Preisach model; then, mapping is trained using LSSVM. This construction provides a complete memory for hysteresis and avoids an accumulation of feedback errors in the inputs. Including the stop operator with the derivative of input in the LSSVM model supports the model to deal with rate-dependent hysteresis, which means that the output displacement depends on input voltage and input frequency (or input rate) and thus has a great generalization ability to model piezoelectric actuators. In addition, the learning capabilities of LSSVM are improved by a Particle Swarm Optimization (PSO) algorithm [37] which has a strong ability to search for the global optimal solution. Based on the hysteresis model and its inversion, a feedforward control strategy is used to compensate hysteresis effect in which LSSVM is trained inversely. Then, a further enhancement of the reference tracking performance is achieved by inserting a PID controller (Incremental PID) into the control loop. Different datasets are applied on a nanopositioning platform for the performance evaluation of the proposed method. The contributions of this study are listed below:

1. This paper presents a generalized LSSVM model to characterize the rate-dependent hysteresis of the piezo-actuated stage. This objective is achieved using a hysteresis memory combined with a kernel-based learning method (LSSVM) optimized by PSO. The hysteresis memory is used to solve the problem of hysteresis mapping and LSSVM is used as a density function estimator.
2. This paper presents a hysteresis compensator that can provide accurate position tracking with less execution time; reaching the second objective depends on achieving the first as well as the capability of the PID controller to minimize residual errors.
3. This paper evaluates the proposed approach using a nanopositioning platform.

2. Hysteresis Modeling with the LSSVM

In this section, the main concept of the proposed method for hysteresis modeling is presented, containing details about hysteresis mapping, hysteresis modeling, and hyper-parameter optimization methods.

2.1. Least-Squares Support-Vector Machine

The support-vector machine (SVM) is one of the most common machine learning techniques used for classification and regression [38]. In regression, SVMs predict model outputs using an ϵ -insensitive loss function, its error is minimized by an optimization algorithm. In this paper, a revised version of SVM, called LSSVM, was used [27,39,40]. LSSVM utilizes equality constraints instead of inequality constraints and squared loss

function instead of the ε -insensitive loss function. This modification simplifies the problem and solves linear equations instead of quadratic programming used in SVM, thus making it better than SVM in terms of accuracy and computation time. Therefore, it has been successfully applied to solve regression problems in many applications. The algorithm of LSSVM regression can be described as follows:

Let us assume a piezoelectric hysteresis model takes the form:

$$y(z) = w^T \varnothing(z) + b \quad (1)$$

and assume the model is trained by the dataset $\{z^k, y_k\}_{k=1}^N$ with N samples, $\varnothing(\cdot)$ represents a nonlinear mapping function that maps input space into multidimensional space, w represents weight vector and b represents bias. The optimal parameters of w and b can be obtained by solving the following optimization problem:

$$\min_{w, e, b} J_p(w, e) = \frac{1}{2} w^T w + C \frac{1}{2} \sum_{k=1}^N e_k^2 \quad (2)$$

subject to:

$$y_k = w^T \varnothing(z^k) + b + e_k \quad (3)$$

where C denotes the regularization parameter. The Lagrangian function is used to solve this optimization problem and find the extreme values as follows:

$$\mathcal{L}(w, b, e; \alpha) = J_p(w, e) - \sum_{k=1}^N \alpha_k [w^T \varnothing(z^k) + b + e_k - y_k] \quad (4)$$

where α_k are the Lagrange multipliers. The optimal solutions can be obtained by using Karush–Kuhn–Tucker (KKT) conditions which can be formulated as follows:

$$\frac{\partial \mathcal{L}}{\partial w} = 0 \rightarrow w = \sum_{k=1}^N \alpha_k \varnothing(z^k) \quad (5)$$

$$\frac{\partial \mathcal{L}}{\partial e_k} = 0 \rightarrow \alpha_k = C e_k \quad (6)$$

$$\frac{\partial \mathcal{L}}{\partial b} = 0 \rightarrow \sum_{k=1}^N \alpha_k = 0 \quad (7)$$

$$\frac{\partial \mathcal{L}}{\partial \alpha_k} = 0 \rightarrow w^T \varnothing(z^k) + b + e_k - y_k \quad (8)$$

by combining Equation (4) and KKT equations, the solutions are obtained as a set of linear equations as follows:

$$\begin{bmatrix} 0 & 1_N^T \\ 1_N & \Omega + I/C \end{bmatrix} \begin{bmatrix} b \\ \alpha \end{bmatrix} = \begin{bmatrix} 0 \\ y \end{bmatrix} \quad (9)$$

where $1_N = [1, 1, \dots, 1]^T$, $y = [y_1, y_2, \dots, y_N]^T$, I is an identity matrix and the Gram matrix is represented as:

$$\Omega_{kj} = K(z^k, z^j) = \varnothing(z^k) \varnothing(z^j), \quad k, j = 1, 2, \dots, N \quad (10)$$

where K is the kernel function. In this study, we used the radial base function (RBF) kernel, which corresponds to:

$$K(z, z^k) = \exp\left(-\frac{\|z - z^k\|}{\sigma^2}\right) \tag{11}$$

where σ is the kernel parameter. Therefore, the LSSVM regression function is derived as:

$$\hat{y}(z) = \sum_{k=1}^N \alpha_k K(z, z^k) + b \tag{12}$$

2.2. LSSVM Hysteresis Model Based on Hysteresis Operator

The idea, in this paper, is inspired by the Preisach model, which has been widely used to represent hysteresis nonlinearity. The Preisach model has been proposed at the end of the last century to represent hysteresis behavior and then developed by including relay operators to represent the rate-independent [41,42]. The relay operator is usually characterized by a pair of thresholds, a_1 and a_2 , where $a_1 \leq a_2$, as shown in Figure 1a, where its output takes a value equal to +1 or -1. The details of the Preisach model are introduced as follows:

Assume that a piezoelectric actuator is driven by a given input voltage $z(t)$, its output can be represented by the Preisach model as follows:

$$y(t) = \int_0^{+\infty} \int_{-\infty}^{+\infty} \mu(r, s) R_{s-r, s+r}[z](t) ds dr \tag{13}$$

where μ is the density function, $R_{s-r, s+r}[\cdot]$ is the hysteresis relay operator, r is the half-width value of the relay operator which is determined by a_1 and a_2 , where $r = (a_2 - a_1)/2$, and s is the mean value of the operator. The half-plane $r > 0$ is separated into two distinct regions using a dividing curve $\psi(t, r)$ so that the relay takes either the value of -1 (in the upper region) or +1 (in the lower region). This curve can be described as a play operator, as shown in Figure 1b, where:

$$\psi(t, r) = P_r[z](t) \quad \forall r \geq 0 \tag{14}$$

Equation (13) can be rewritten as:

$$y(t) = \int_0^{+\infty} \left[\int_{-\infty}^{\psi(t, r)} \mu(r, s) ds - \int_{\psi(t, r)}^{+\infty} \mu(r, s) ds \right] dr \tag{15}$$

and thus, the Preisach hysteresis model can be expressed as:

$$y(t) = Q(r, \psi(t, r)) \tag{16}$$

as can be seen from Equation (16), the Preisach model contains two parts; a hysteresis memory defined as a continuous set of play operators, and a memoryless functional defined by a single-to-single mapping function. The most important challenge in the Preisach model is how to approximate the density function μ by more accurate methods and the process should be less time-consuming. To address these issues, various approaches have been proposed in the literature. One of the most effective ways is to use a Discrete Preisach Model with neural networks, in which the Preisach plane is first divided into a finite number of intervals (cells); then the density function is approximated by artificial neural networks (NN) [19,43]. Although the results demonstrated that ANN-based methods were successful, ANNs are based on the principle of empirical risk minimization, thus they are prone to overfitting problems and low generalization ability.

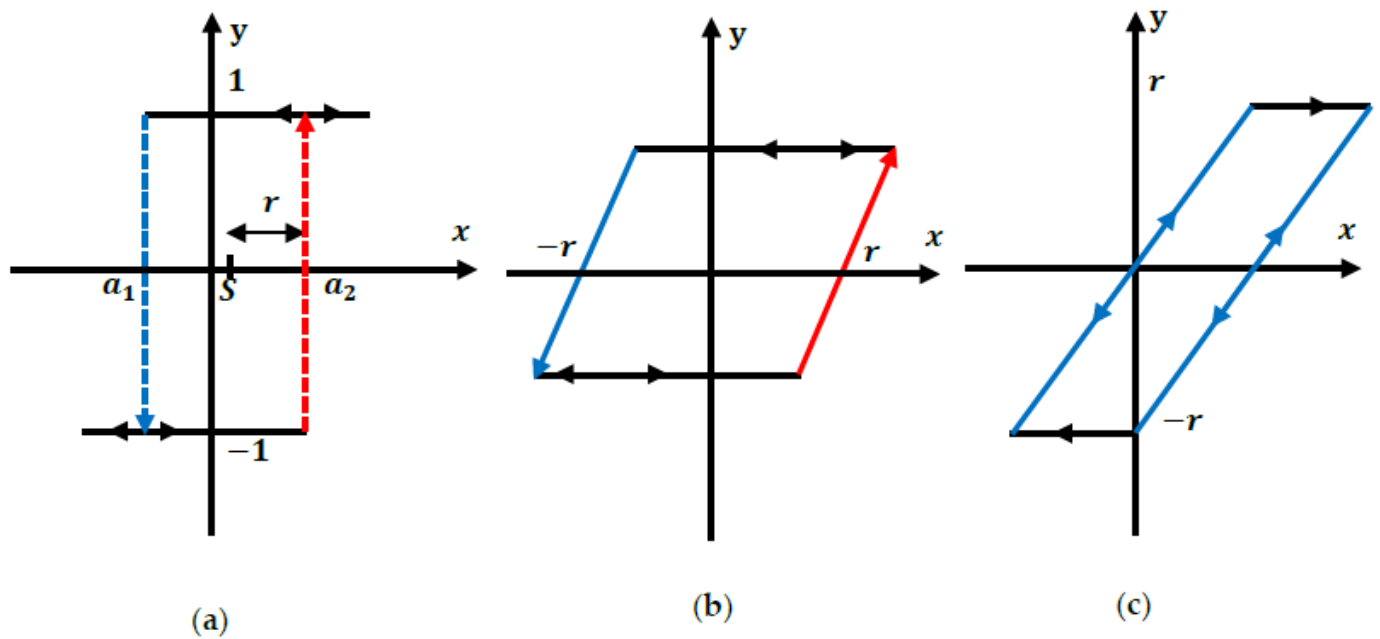


Figure 1. Representation of hysteresis operator of Preisach model: (a) Relay operator; (b) play operator; (c) stop operator.

In this study, an alternative approximation strategy was assessed on a piezoelectric actuator for a nanopositioning system, where the LSSVM model was tested according to its ability to approximate the mapping function. Figure 2 illustrates the proposed model architecture. The hysteresis memory was constructed in a discrete form using a set of n stop operators, and then the memoryless mapping function was identified by an LSSVM-based regression model. The stop operator can be described, as indicated in Figure 1c, with two thresholds $+r$ and $-r$. The output of the stop operator can be mathematically expressed on each subinterval $[t_i, t_{i+1}]$ for the input $x(t)$, where $0 = t_0 < t_1 < \dots < t_N$, as follows:

$$z(0) = E_r[x(0)]$$

$$z(t) = E_r[x(t) - x(t_i) + z(t_i)] \tag{17}$$

for $t_i \leq t \leq t_{i+1}; 0 \leq i \leq N - 1$

where:

$$E_r[\cdot] = \min\{\max\{-r, \cdot\}, +r\} \tag{18}$$

where $E_r[\cdot]$ is the stop operator, and $z(t)$ is the current state of the stop [42]. The threshold is determined by the following formula:

$$r_i = \frac{i}{(n + 1)|x|_{max}}, \quad i = 1, 2, 3, \dots, n \tag{19}$$

where $|x|_{max}$ is the maximum absolute value of the input $x(t)$ and n is the number of stop operators which can directly affect the model’s accuracy and its complexity. The high capability of generalization and learning of the proposed model comes from the following:

1. The classical Preisach hysteresis model is rate-independent, which means that the output displacement depends only on input voltage and not input frequency (or input rate) [7]. The proposed method of LSSVM makes it possible to deal with rate-dependent and thus have a great generalization ability to model piezoelectric actuators. For this purpose, we included the input signal $x(t)$ and the input rate $\dot{x}(t)$ in

the LSSVM model. The values of $x(t)$ were calculated using the backward difference formula [44].

2. We used the stop operators to gain a more detailed description of the characteristics of the hysteresis loop, thus locating the model response as close as possible to the experimental results. Additionally, the hysteresis multivalued mapping is converted into a single-to-single valued mapping without feedback which accumulates errors over time, as in LSSVM-NARX.
3. We used a very effective search technique, called Particle Swarm Optimization (PSO) [37], to set the appropriate values of hyper-parameters α and C . The PSO has been successfully used to tune the LSSVM parameters in diverse fields and both simulation and experimental results showed that the PSO algorithm enhanced the accuracy of the models and improved the generalization ability of the LSSVM model [31,45,46]. The details of the PSO algorithm will be discussed in the next subsection.

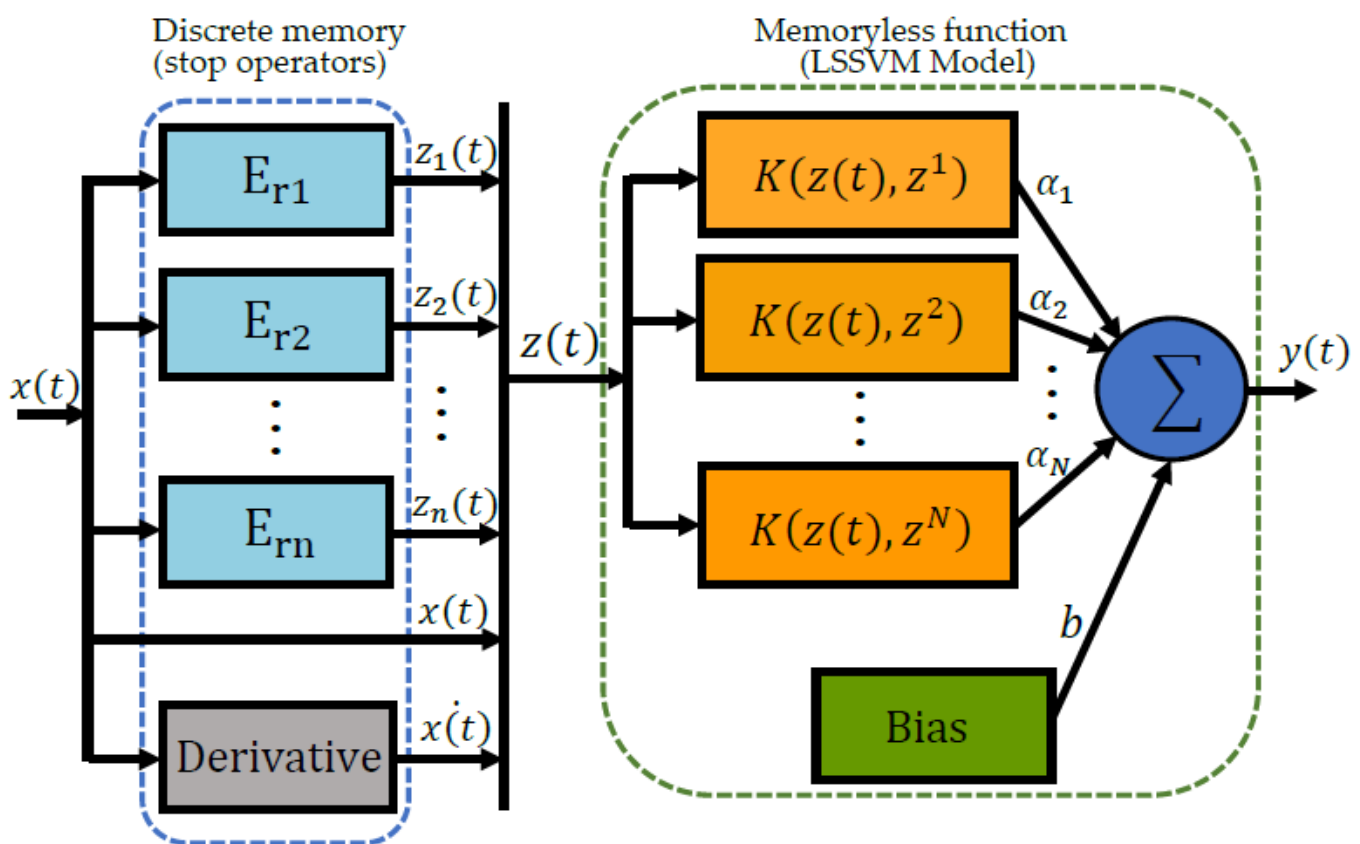


Figure 2. Structure of the proposed LSSVM hysteresis model.

The LSSVM model is trained with a dataset containing the input vector $z(t)$ and the output displacement $y(t)$, where $z(t) = [z_1(t) z_2(t) \dots z_n(t) x(t) \dot{x}(t)]$, and n is the number of stop operators. A description of the input signals applied to the piezoelectric actuator will be presented later. Simulations in this work have been implemented using MATLAB/Simulink (version R2021b, Mathworks, Natick, MA, USA) and with the help of the LS-SVMlab Toolbox (version 1.8, KU Leuven, Leuven, Belgium) [47].

2.3. Optimization of LSSVM Parameters Based on PSO

The strategy of tuning hyper-parameters C and σ plays a significant role to enhance the accuracy of the LSSVM model. To this purpose, PSO is used in this study to optimize the hyper-parameters. The basic idea of the PSO algorithm was inspired by the movement of a bird swarm while searching for food [37,48]. The movement of each particle in D-

dimensional search space is controlled via the inter-communications among them to find the best position for food. In every iteration, each particle follows the nearest one to the food until reaching the most optimal, which is the final, solution. This intelligent scenario makes the PSO algorithm acts as a powerful tool in optimization problems. Every particle in the swarm is specified by its current position and velocity information which are updated in every iteration. The following formulas describe how the position and velocity are updated for a particle i at iteration t in D-dimensional search space:

$$\begin{aligned} v_i(t) &= \eta v_i(t-1) + c_1 r_1 (p_{best,i} - p_i(t-1)) + c_2 r_2 (g_{best} - p_i(t-1)) \\ p_i(t) &= p_i(t-1) + v_i(t) \end{aligned} \quad (20)$$

where $p_i(t)$ and $v_i(t)$ are the current position and the current velocity, respectively, η is the inertia weight, $p_{best,i}$ is the current personal best, g_{best} is the current global best, c_1 and c_2 are individual and group learning rates, and r_1 and r_2 are uniformly distributed random numbers in the range $[0, 1]$. In this study, cross-validation was used to evaluate the performance of each particle, which measures the error between actual and predicted outputs. The detailed steps of the PSO-based LSSVM algorithm are thus given as follows:

1. Set the parameters of PSO, take the parameters σ and C as swarms, and randomly initialize the position and velocity of each particle.
2. Initialize parameters of LSSVM, train the LSSVM model and then test and evaluate objective values of each particle based on cross-validation.
3. Find personal best and global best. Particle i replaces personal best if it is superior and best particle replaces global best if it is superior.
4. Update the position and velocity of each particle as shown in Equation (20).
5. Repeat steps 2 and 3 until the maximum number of iterations or the optimum solution (minimum error) is reached.

3. Experimental Setup and Modeling Results

This section provides a brief description of the platform used in experiments and discusses the validation results of the proposed model.

3.1. Experimental Setup

All experiments were carried out on a piezo-actuated nanopositioning platform for the performance evaluation of the proposed approach. As shown in Figures 3 and 4, the experimental environment includes the following components:

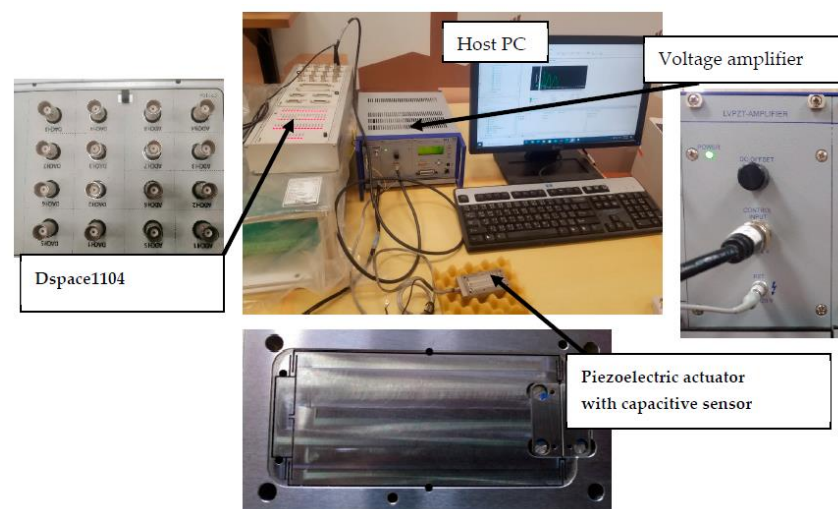


Figure 3. The nanopositioning system experimental setup.

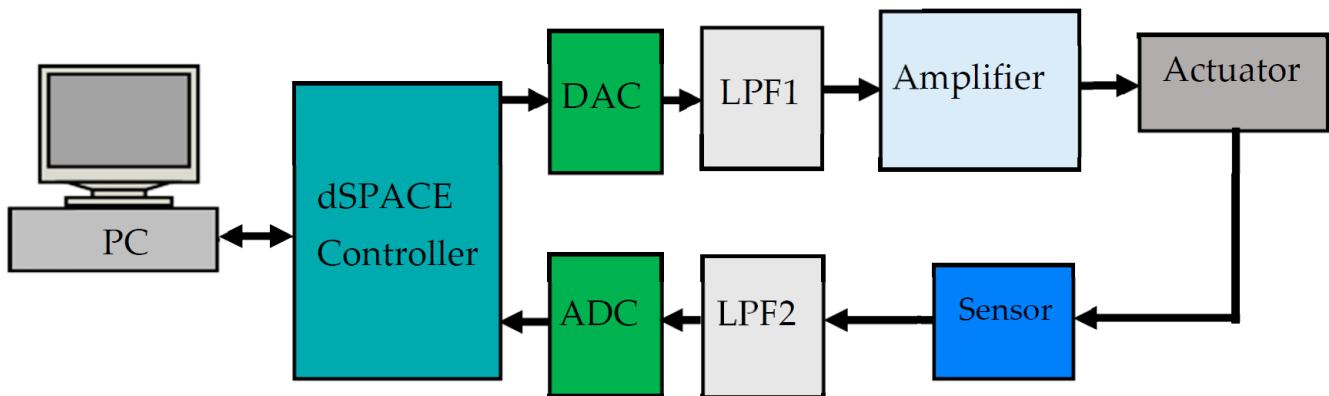


Figure 4. Scheme diagram of the experimental setup of the nanopositioning system.

- **Nanopositioning stage:** A single-axis high-precision piezoelectric stage (P-752.21C, manufactured by Physik Instrumente Company, Karlsruhe, Germany) [49] was used. This stage contains a flexure-hinge-guided mechanism driven by a piezoelectric stack actuator as well as a capacitive sensor, as shown in Figure 5. The flexure-hinge-guided mechanism provides motion through elastic deformations, as there are no sliding parts, thereby avoiding undesired nonlinear effects, such as backlash and friction. The piezoelectric stack actuator is composed of several layers of piezoelectric materials connected mechanically in series and wired electrically in parallel. Each layer is made of a piezoelectric ceramic material (PICMA[®] P-885) which converts an electrical signal into displacement and generates a force on the mechanism. The actuator expands and contracts according to the sign of the applied voltage, V . The considered piezoelectric actuator has a travel range of up to $35\ \mu\text{m}$, a $0.1\ \text{nm}$ displacement resolution, and can be driven in the -20 to 120 voltage range. The displacement is measured by the capacitive sensor (D-015) which has an extended measuring range of $45\ \mu\text{m}$ and can provide a subnanometer resolution ($0.01\ \text{nm}$). This sensor has high bandwidth ($10\ \text{kHz}$) and produces an analog output voltage in the range of 0 to $10\ \text{V}$. Table 1 presents the specifications of the considered piezo-actuated nanopositioning stage. These characteristics of the piezoelectric stage make it suitable for high-speed precision actuation.
- **Piezo Amplifier Module:** A voltage amplifier (E-505.00, manufactured by Physik Instrumente Company, Germany) [50] with a fixed gain of 10 was used to amplify the control signal and drive the piezoelectric actuator. The bandwidth of this amplifier is $3\ \text{kHz}$, and it can operate in the input voltage range from -2 to $+12\ \text{V}$ and produce output voltages ranging from -30 to $+130\ \text{V}$.
- **Control Board:** The control algorithms were executed on the dSPACE1104 board (DS1104, dSPACE Inc., Wixom, MI, USA) [51] which allows a perfect real-time execution of the control algorithms on hardware-in-the-loop simulation (HILS). The dSPACE1104 is popular in academic engineering research and particularly well-suited for prototyping control systems [52–54]. It provides many advantages in terms of speed and precision which can allow extended algorithms to be practically implemented in real-time, as it is equipped with a $250\ \text{MHz}$ processor (MPC8240) with $32\ \text{MB}$ of SDRAM and $8\ \text{MB}$ of flash memory. The input control signals and output displacements of the piezoelectric actuator are sent from/to the dSPACE controller via a built-in A/D converter, D/A converter, and the dSPACE CLP1104 connector which has 16 BNC ports. The input voltage range is from -10 to $+10\ \text{V}$ on eight A/D conversion ports with 16 bits of resolution for the first four ports and 12 bits of resolution for the remaining ports. The board also includes low-pass filters to avoid aliasing effects. The cutoff frequency is set at $40\ \text{Hz}$. The dSPACE1104 is directly connected with a PC that executes the control simulation.

- **Development Computer:** The host computer includes Matlab Real-time Interface (RTI) and ControlDesk. The RTI is MATLAB-Simulink software used to create the control part and generate a real-time C-code. The ControlDesk contacts the C-code for real-time measurement and visualization.

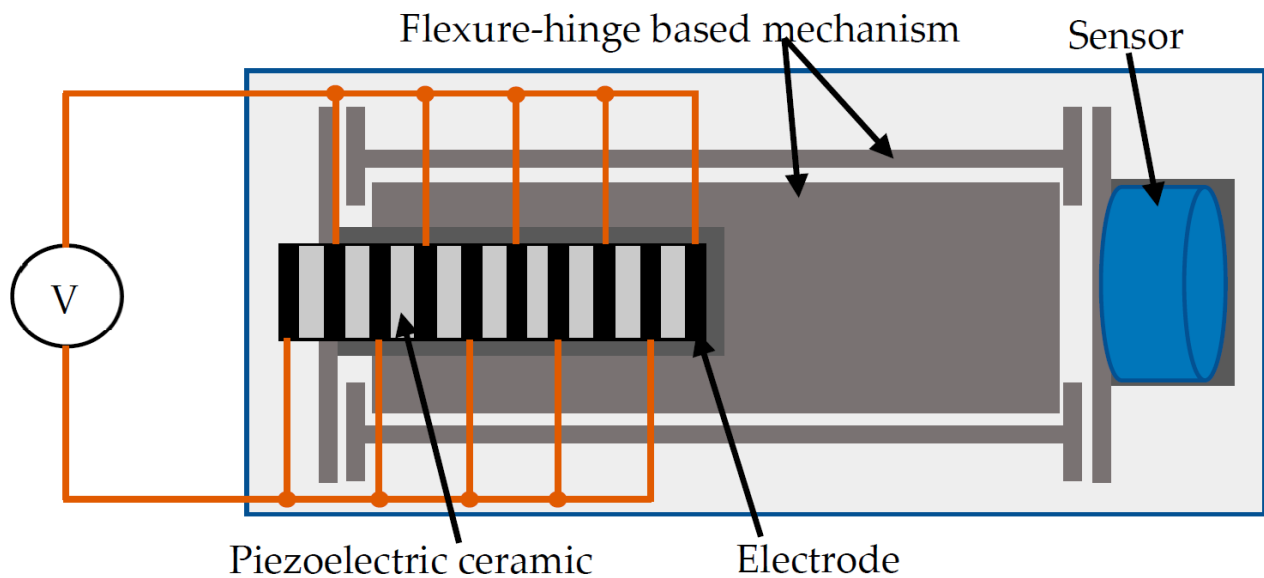


Figure 5. The basic elements of the piezoelectric stack stage.

Table 1. Specification of the considered piezoelectric actuator.

Properties	Values
Driven input voltage (V)	−20 to 120
Resonant frequency (Hz)	2100
Resolution (nm)	0.1
Travel range (μm)	0–35
Stage mass (kg)	0.35
Electrical capacitance (μF)	3.7
Load capacity (N)	30
Stiffness in motion direction ($\text{N}/\mu\text{m}$)	20

3.2. Modeling Results

For proper modeling of hysteresis, the training datasets have to be thoughtfully designed to include various hysteresis loops for different frequencies. The training and test data should include the rate-dependent and rate-dependent hysteresis loops. Therefore, in this study, the piezoelectric actuator was excited by different input signals in the range of 1 to 20 Hz which include the rate-dependent and rate-dependent hysteresis loops. The sampling rate for each input signal is 0.002 s. Seven input signals were used, as shown in Figure 6, where three of which were used for training and four for testing. In addition, as mentioned in Section 3.1, the considered piezoelectric actuator can only be driven in the −20 to 120 voltage range so that the voltage at the reference input should be less than 12 V, which is then amplified by a fixed gain of 10. A higher voltage at reference input results in oscillations which can cause irreparable damage to the piezo actuator. Accordingly, the maximum input voltage considered in this study is 8.5 V. Table 2 lists detailed information about these datasets. The experimental data obtained were then used for the identification and validation of the proposed model. The corresponding hysteresis loops under the training and test input signals were generated as shown in Figure 7, it can be noticed that these loops include rate-independent and rate-dependent hysteresis by which the generalization ability of the proposed model was examined in this study. To measure their

effect on performance, the Root Mean Square of Error (RMSE) [55] was calculated for the given training and test datasets A, B, C, D, E, F, and G, and was 1.7466 μm , 2.0566 μm , and 0.8623 μm , 1.7708 μm , 0.7140 μm , 0.4443 μm , and 5.8008 μm , respectively. This accounts for 4.990%, 5.876%, 2.463%, 5.059%, 2.040%, 1.2695%, and 16.5736% of the travel range, respectively, thus it is necessary to achieve accurate modeling and control.

All simulations were performed with the sampling rate of the input signals (0.002 s), one second for each input signal, meaning that the number of samples was 500 for each. The maximum absolute value of the input $x(t)$ (this is a parameter for the stop operator) was set to 8.5. LSSVM hysteresis model was trained with 55 stop operators on the given training data, as well as the input $x(t)$ and the input rate $\dot{x}(t)$, thereby the order of the LSSVM model is 57. For the sake of comparison, we first adopted the 5-fold cross-validation method to optimize the hyper-parameters based on Coupled Simulated Annealing (CSA) [56] and the simplex method [57]. The CSA was used to initially determine proper initial starting values and the simplex method uses these values to find more optimal parameters. The obtained optimized hyper-parameter values (C and σ^2) were 3.0450×10^7 and 6.5814, respectively. These parameters were then used to train the model to obtain the bias b and the support values α_k . The obtained bias value was 1.389 and the features of the support-vector were sufficient to make a prediction close to the actual output. Table 3 shows a list of simulation parameters. In this study, we use proposed model (1) as a name for the model that uses the optimization method mentioned above and proposed model (2) for the model based on the PSO technique. Figure 8a–c compares the results of the trained proposed model (1) with the experimental data, it can be noted that proposed model (1) shows a good performance for the piezoelectric hysteresis under different sinusoidal and random signals. This model was also tested on the test data; D, E, F, and G; Figure 8d–g shows the corresponding hysteresis loops compared with the experimental data. The Root Mean Square of Error (RMSE) was also used to evaluate proposed model (1) for training and test data. The RMSEs for training samples A, B, and C were 0.0326 μm , 0.1146 μm , and 0.0047 μm , respectively. In addition, it was tested by D, E, F, and G data where it produced RMSEs of 0.0193 μm , 0.0316 μm , 0.0176 μm , and 0.033 μm , respectively, which account for 0.055%, 0.090%, 0.050%, and 0.094% of the travel range.

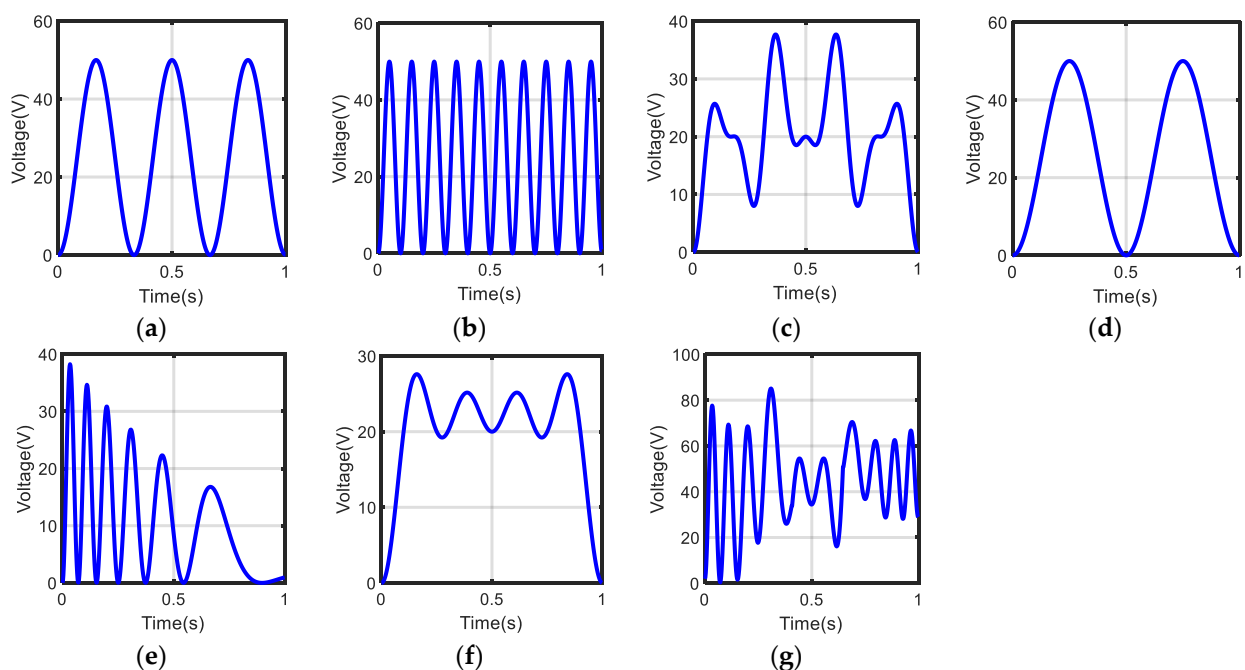


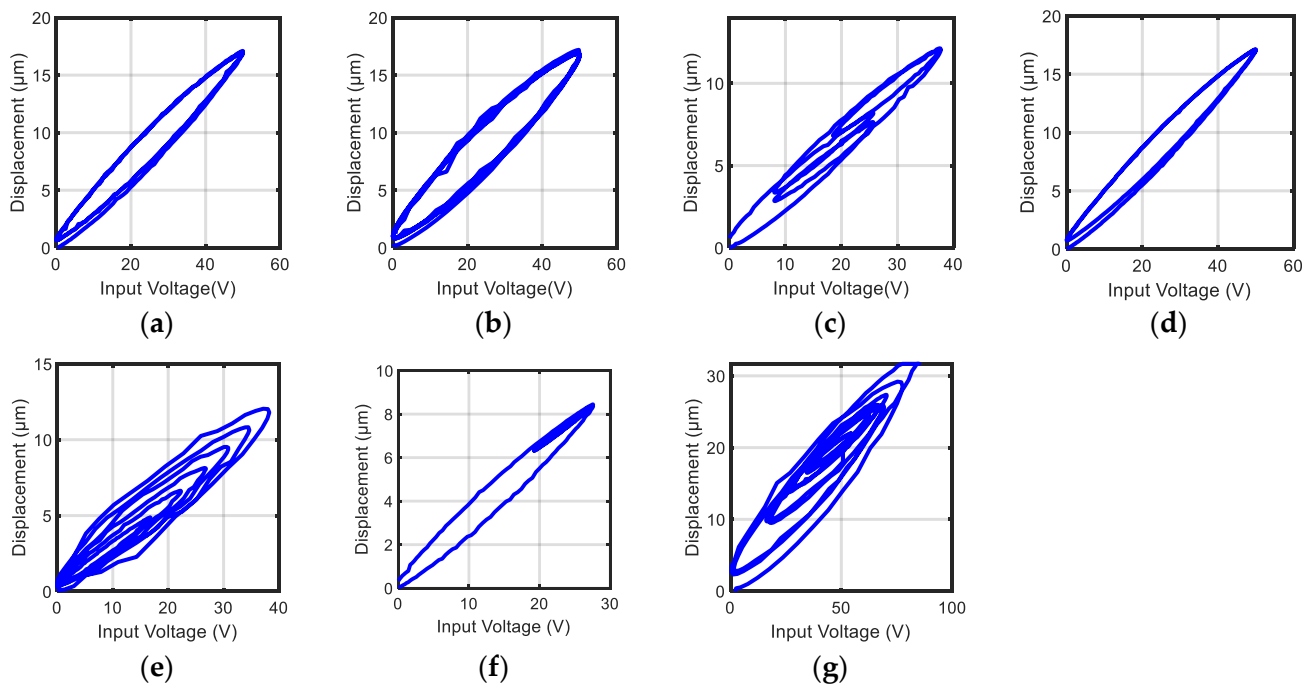
Figure 6. Datasets: (a) training input A; (b) training input B; (c) training input C; (d) test input D; (e) test input E; (f) test input F; (g) test input G.

Table 2. Description of training and testing data.

Signal	Information	Frequency
A	$x(t) = 2.5\sin(6\pi t - \pi/2) + 2.5$	3 Hz
B	$x(t) = 2.5\sin(20\pi t - \pi/2) + 2.5$	10 Hz
C	Random sinusoidal	1–7 Hz
D	$x(t) = 2.5\sin(4\pi t - \pi/2) + 2.5$	2 Hz
E	$xt = 2e^{-0.13t}[\cos(3\pi te^{-0.09t} - 3.15) + 1]$	1–20 Hz
F	Random sinusoidal	1–5 Hz
G	Random sinusoidal	1–20 Hz

Table 3. Summary of simulation parameters.

Parameter	Value
No. of samples (N)	500 for each data
Sampling rate	0.002 s
The maximum input ($ x _{max}$)	8.5
Cross-validation	5
Model input order	57
Regularization factor (C)	3.0450×10^7
Kernel sample variance (σ^2)	6.5814
Bias (b)	1.389

**Figure 7.** Hysteresis loops generated by: (a) input voltage A; (b) input voltage B; (c) input voltage C; (d) input voltage D; (e) input voltage E; (f) input voltage F; (g) input voltage G.

For comparison, the classical Preisach and LSSVM-NARX models were also trained on the same given training data. The Preisach plane was discretized into n discrete intervals (cells) to numerically approximate the density function, as already used in a previous study [38,39,58–60]. Higher discretization levels increase the model order, making the computational implementation of the Preisach model more time-consuming. In this study, we evaluated the Preisach model at different levels of discretization; 50, 100, and 120, which account for 1275, 5050, and 7260, respectively, of Preisach elements n . The formula

for calculating the number of Preisach elements is given as $n = (L(L + 1))/2$, where L is the level of discretization. In our study, the LSSVM-NARX model was trained by introducing current and past inputs and past output displacements to estimate current output displacements. According to a previous study [59], it has been found that the increase in the order of the LSSVM-NARX model increases its accuracy in training, but also increases the computational complexity. Additionally, the different selections of order do not monotonically affect the resulting modeling accuracy in test samples. As a compromise, the authors recommended that both n and m are set to 3. That is:

$$z_k = [x_k \ x_{k-1} \ \dots \ x_{k-n} \ y_{k-1} \ \dots \ y_{k-m}] \tag{21}$$

where $n = m = 3$.

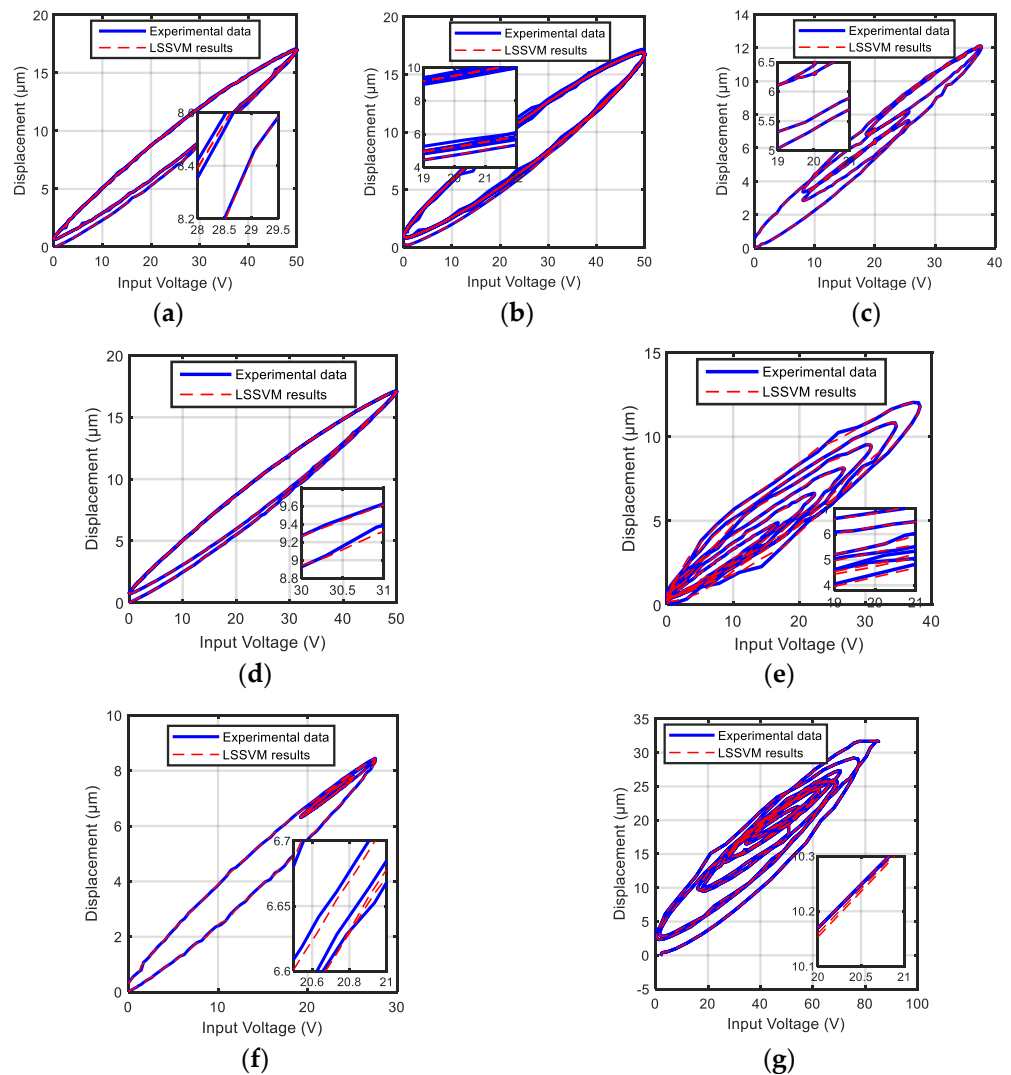


Figure 8. Simulation results of proposed model (1) on: (a) training data A; (b) training data B; (c) training data C; (d) test data D; (e) test data E; (f) test data F; (g) test data G.

Figures 9 and 10 and Table 4 show the error between the actual output of the actuator and the simulation output of proposed model (1) and those obtained by the classical Preisach and LSSVM-NARX models for test data D, E, F, and G. The results demonstrate that the LSSVM based on the hysteresis operator is superior and more accurate in terms of RMSE (0.0193, 0.0316, 0.0176, and 0.033 μm , respectively) than the classical Preisach and the LSSVM-NARX models. The LSSVM-NARX model presents better results than the Preisach model for all data. It can be also seen the accuracy of the Preisach model increases with

increasing its order, but the computation time increases. It was also found that proposed model (1) is less time-consuming (nearly 7 times) than the Preisach (with $n = 7260$) which gives the highest accuracy. Although proposed model (1) requires more time (nearly five times) than the LSSVM-NARX model, its high accuracy and reasonable computation time make it more advantageous to provide a real-time tracking control of the piezoelectric actuator compared to all other models considered in this paper.

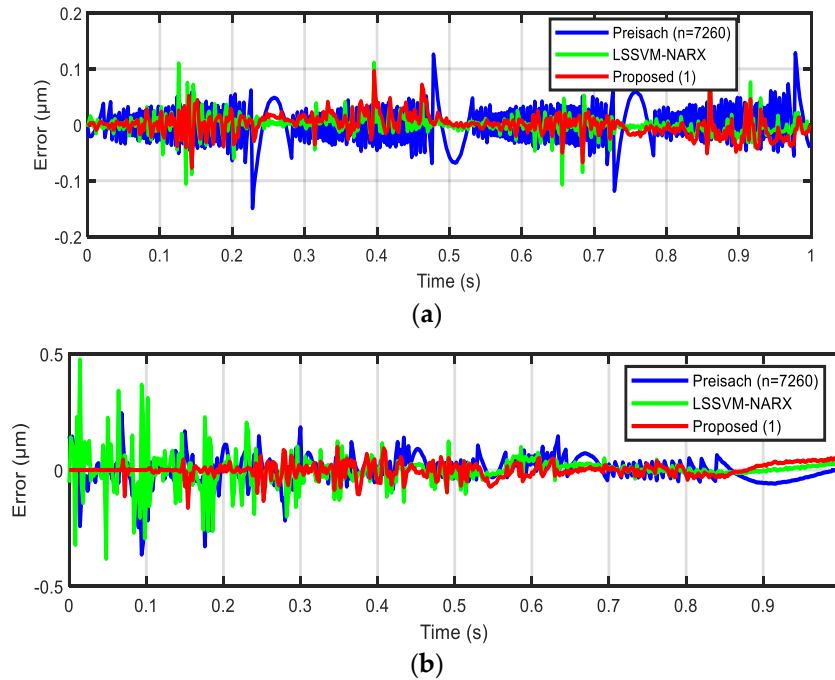


Figure 9. The error between the actual output of the actuator and the simulation output of proposed model (1) and the comparative models for: (a) test data D; (b) test data E.

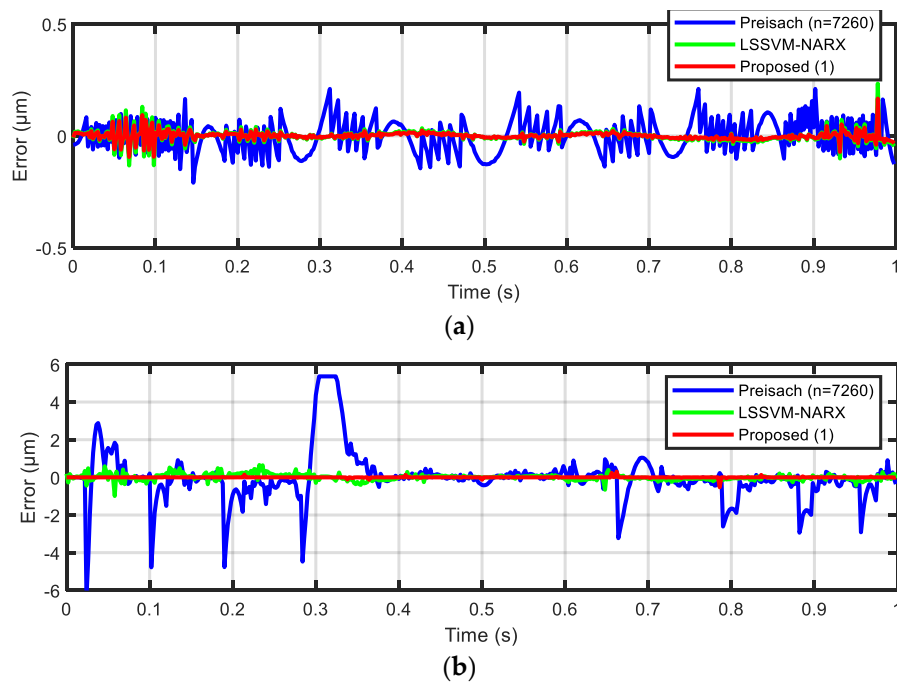


Figure 10. The error between the actual output of the actuator and the simulation output of proposed model (1) and the comparative models on (a) test data F; (b) test data G.

Table 4. Comparison of modeling results with Preisach and LSSVM-NARX models.

Model	RMSE (μm)				Average Computation Time per One Test Sample (ms)
	Data D	Data E	Data F	Data G	
Preisach ($n = 1275$)	0.2508	0.2941	0.2512	1.3620	0.25
Preisach ($n = 5050$)	0.1198	0.1996	0.1289	1.3443	1.14
Preisach ($n = 7260$)	0.0803	0.1779	0.0737	1.3367	1.62
LSSVM-NARX	0.0208	0.0718	0.0254	0.1660	0.05
Proposed model (1) ($n = 55$)	0.0193	0.0316	0.0176	0.0330	0.23

Although the results show good performance of proposed model (1), the hysteresis should be more accurately identified, especially for training samples B and the test samples E and G. This may be because the optimization problem needs a stronger search capability to find optimal hyper-parameters C and σ , or the proposed model requires higher levels of discretization to provide a higher degree of accuracy. To investigate these hypotheses, the PSO algorithm was first proposed and evaluated to optimize the hyper-parameters, and then the effect of the number of stop operators on the model's performance was examined.

Some parameters of the PSO should be chosen carefully before the algorithm is applied, which are the population size, the maximum iteration number, the inertia values, and the local and global accelerations. In most applications, the population size is recommended to be in the range of 20–50 [60–62]. The maximum number of iterations is the stopping criterion in the PSO algorithm, and a higher number allows for more accurate tuning but with a high computational cost. A larger value of c_2 indicates that the algorithm evolves quickly, whereas a larger value of c_1 indicates the algorithm evolves slowly and the optimization process may be terminated before reaching the best solution. Therefore, according to previous recommendations [63,64] and based on our experiments, the parameters of the PSO algorithm were set in as follows: the size population is set to 30, and the maximum iteration number is set as 100. The inertia values are 0.9 and 0.4 and $c_1 = c_2 = 2$. Accordingly, the tuning process was conducted, and the best-found hyper-parameters values were $\sigma = 3.13544$ and $C = 3.8155 \times 10^3$. Then, these parameters were used to optimize LSSVM.

Figure 11 compares the simulation results of proposed model (2) with the experimental data. The results showed that proposed model (2) outperformed proposed model (1) on all given data where the RMSEs for datasets A, B, C, D, E, F, and G were 0.01040 μm , 0.00249 μm , 0.003081 μm , 0.01061 μm , 0.01086 μm , 0.0123 μm , and 0.0126 μm , respectively. Figure 12a,b shows the error between the actual output of the actuator and the simulation output of proposed model (1) and proposed model (2). It can be concluded that the PSO algorithm contributed greatly to providing better identification results and enhancing the model's capability for different hysteresis cases.

To evaluate the effect of the number of stop operators on the model performance, different models have been considered, each has a different number of stop operators lying in the range of 20 to 110. This requires retuning the hyper-parameters C and σ . Table 5 shows the optimum hyper-parameters for each n . Figure 13 clearly shows the simulation results in terms of RMSE for a different number of stop operators, the results demonstrate the effect of the number of stop operators on the RMSE in dataset B. It can be noted that the increase in the number of stop operators improves the RMSE of the trained model. However, it should be also noted that the results show only a slight improvement in the RMSE (decreases from 0.00231 to 0.00198 μm) in the range of 28 to 105 stop operators, respectively. As mentioned previously, the higher number of input variables (higher number of stop operators) certainly increases the computation time. Since one of the objectives of this study is to reduce the model complexity and guarantee performance improvement, the correlation between execution speed and accuracy has been investigated in this study. This discussion will be presented later in the next section.

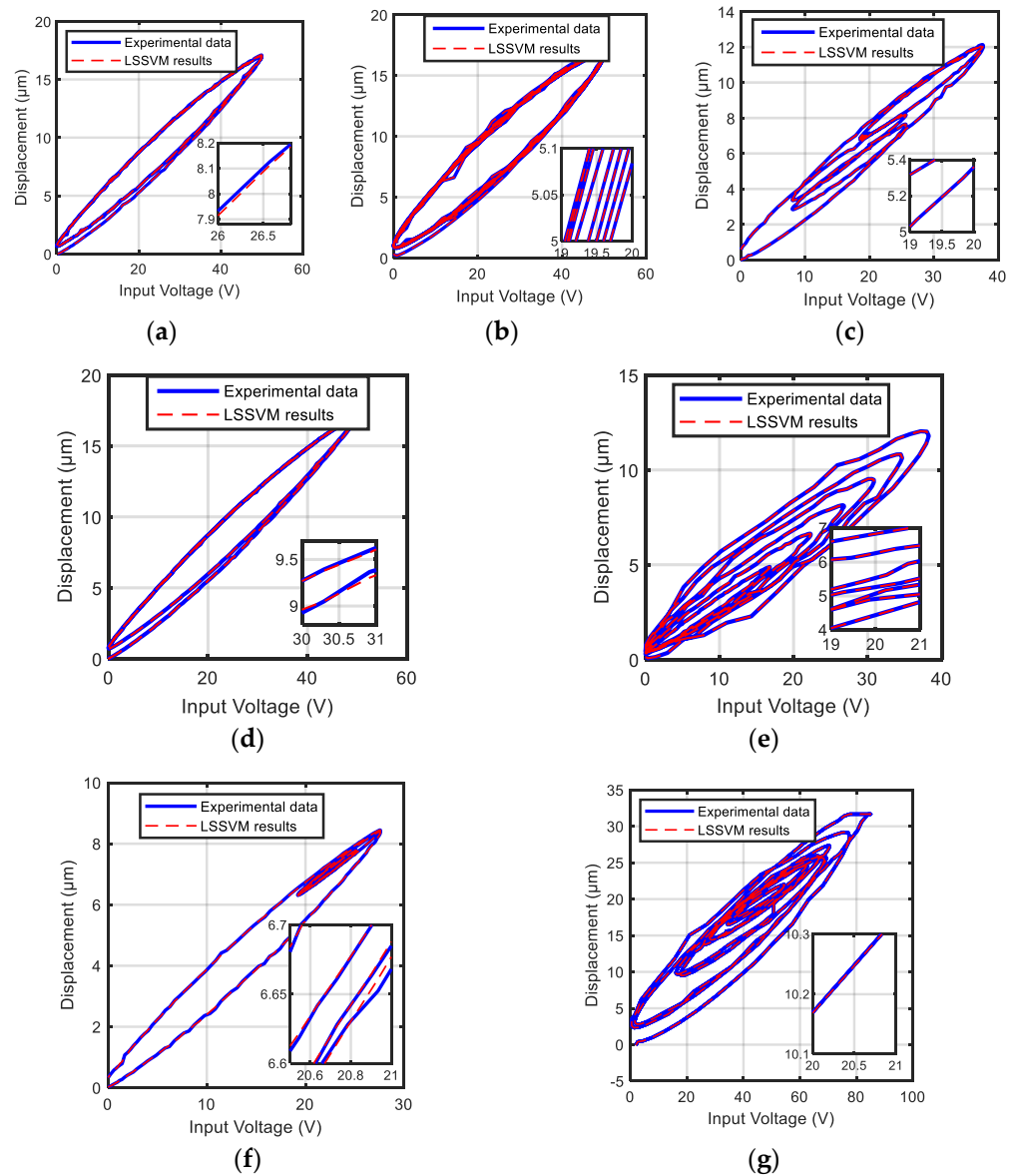


Figure 11. Simulation results of proposed model (2): (a) training data A; (b) training data B; (c) training data C; (d) test data D; (e) test data E; (f) test data F; (g) test data G.

Table 5. The optimum values of hyper-parameters for different numbers of stop operators of proposed model (2).

No. of Stop Operators	Hyper-Parameters of LSSVM Model	
	Ln(C)	σ
21	18.01070	6.62159
28	10.17186	3.69526
36	10.06112	3.68417
55	8.246823	3.13544
78	8.243789	2.94893
91	8.238002	3.31544
105	8.233014	4.02981

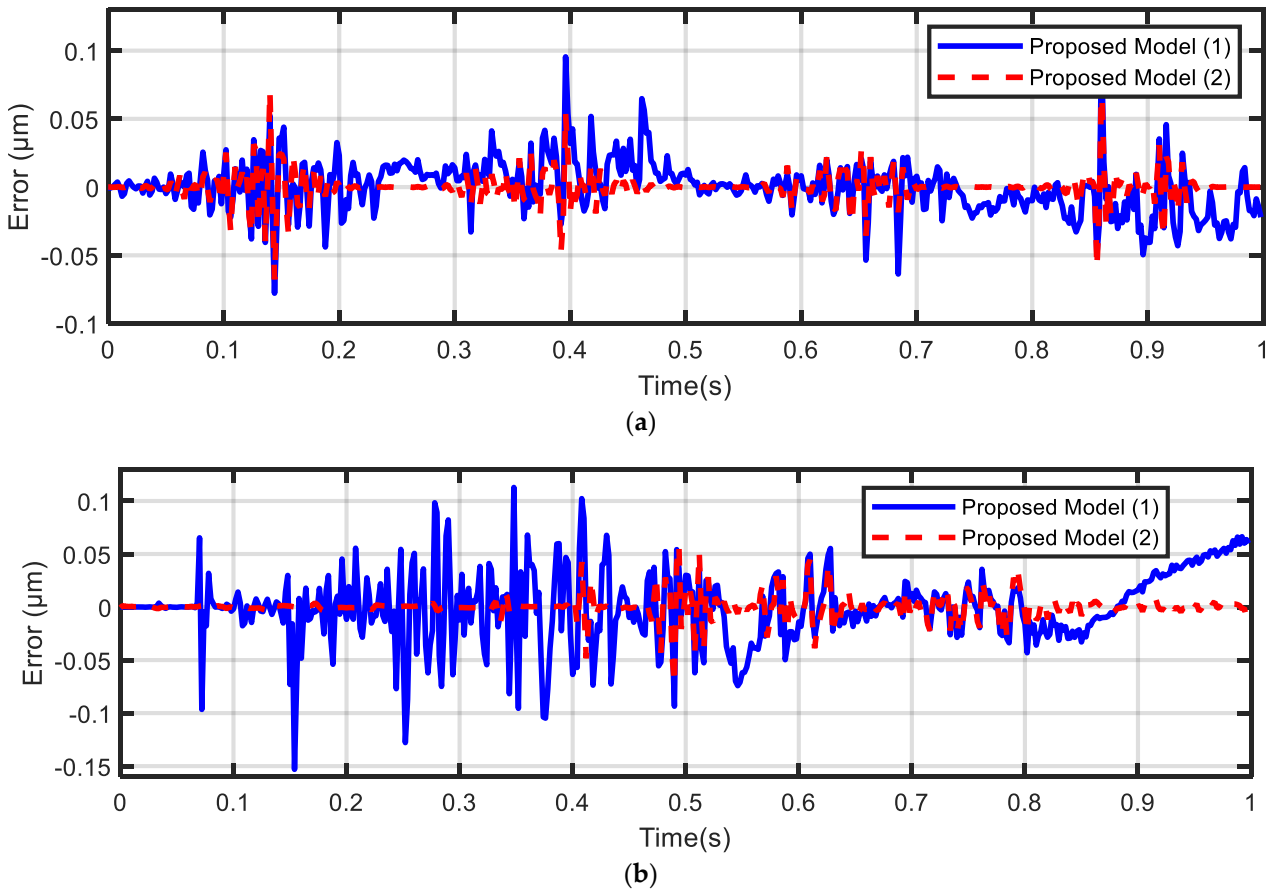


Figure 12. The error between the simulation output and actual output of the actuator of proposed model (1) and proposed model (2) for: (a) test data D; (b) test data E.

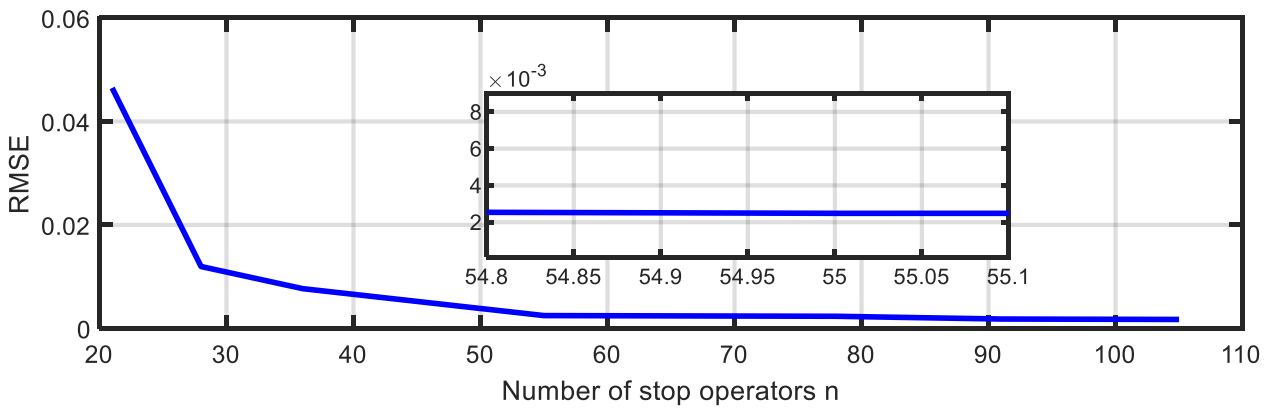


Figure 13. The simulation results in terms of RMSE for a different number of stop operators. The results demonstrate the effect of the number of stop operators on the RMSE on dataset B.

4. Control Design for Piezo-Actuated Nanopositioning Stage

In this section, two control schemes are presented and their performances are evaluated through real-time experiments on the proposed piezo-actuated nanopositioning stage. First, a feedforward (FF) control scheme is proposed for hysteresis compensation, and then it is combined with a feedback (FB) controller to correct for residual errors. Finally, the comparisons of results obtained from these experiments are presented to verify the feasibility and strength of the method proposed in this paper.

4.1. Hysteresis Compensation Using the Inverse LSSVM Model

The high-precision position control of piezoelectric-actuated nanopositioning stages is often a challenging task due to the nonlinear hysteresis effects. The inverse-based control strategies have been widely and successfully applied to control the position of a piezoelectric actuator [5,65]. In this subsection, to compensate for the hysteresis nonlinearity, a feedforward control scheme was designed using the inverse LSSVM model. For this purpose, the model was first trained offline inversely with the given training data where the output displacement was used as the input of the LSSVM model, whereas the input voltage was used as an output. The inverse LSSVM model was then used for the FF control to directly correct the positioning errors online, as shown in Figure 14. The test data D, E, F, and G were employed to evaluate the proficiency of the proposed FF control scheme. Since hyper-parameter tuning algorithms are only required during training, there is certainly no difference in time execution between the two previously proposed LSSVM models. Thus, only one of the proposed models (model 2) was chosen to be used to assess our control scheme. The laboratory results of the FF control are presented in Figure 15. The results show the measured output displacements (the output of the piezoelectric actuator) track the reference (the desired output) precisely as the controller achieves a perfect compensation with RMSEs of 0.0258 μm , 0.0361 μm , 0.0236 μm , and 0.0415 μm , which account for 0.0737%, 0.1031%, 0.0674%, and 0.1186% of the travel range, respectively. These results demonstrate the capability of LSSVM model inversion as well as the effectiveness of the hysteresis operators in compensating the hysteresis nonlinearity and achieving high-precision tracking.

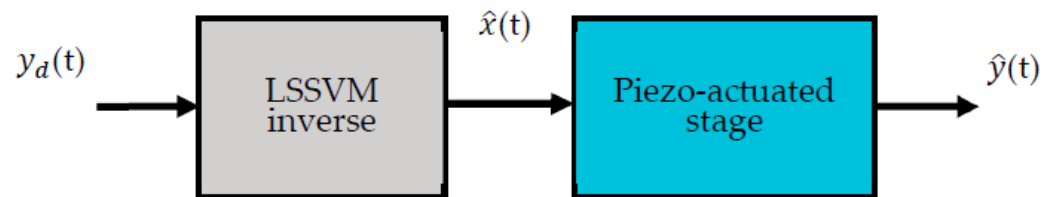


Figure 14. Block diagram of the proposed FF control scheme.

As previously mentioned, the applicability of the proposed control scheme should be examined to determine possible requirements to have both high tracking accuracy and low execution time. Therefore, different control schemes with different numbers of stop operators lying in the range of 20 to 110 (the same range investigated in the modeling stage) have been considered. Table 6 shows the effect of the number of stop operators on the execution time and the RMSE of hysteresis compensation for datasets E. It can be noted that the increase in the number of stop operators resulted in a decrease in the RMSE. However, the control algorithm with $n > 55$ of stop operators cannot be implemented (overrun) within the sample time (2 ms). This error occurs because the LSSVM algorithm is a kernel-based learning method in which the prediction of the output relies on a $(N \times N)$ kernel matrix, where N is the training sample size. Accordingly, the time complexity of the proposed control scheme comes mainly from the increase in the total number of training samples as well as the number of stop operators. Therefore, it can be concluded that the optimal tradeoff between speed and accuracy that guarantees performance improvement is at $n = 55$ and the residual tracking errors can be reduced by combining a FB control with the FF control. This will be discussed in the next subsection.

Table 6. The effect of the number of stop operators on the execution time of control tasks for dataset E.

No. of Stop Operators	Tracking Result RMSE (μm)	Maximum Execution Time (ms)
21	0.0483	0.55
28	0.0456	0.84
36	0.0413	1.21
55	0.0361	1.64
78	overrun condition	
91	overrun condition	
105	overrun condition	

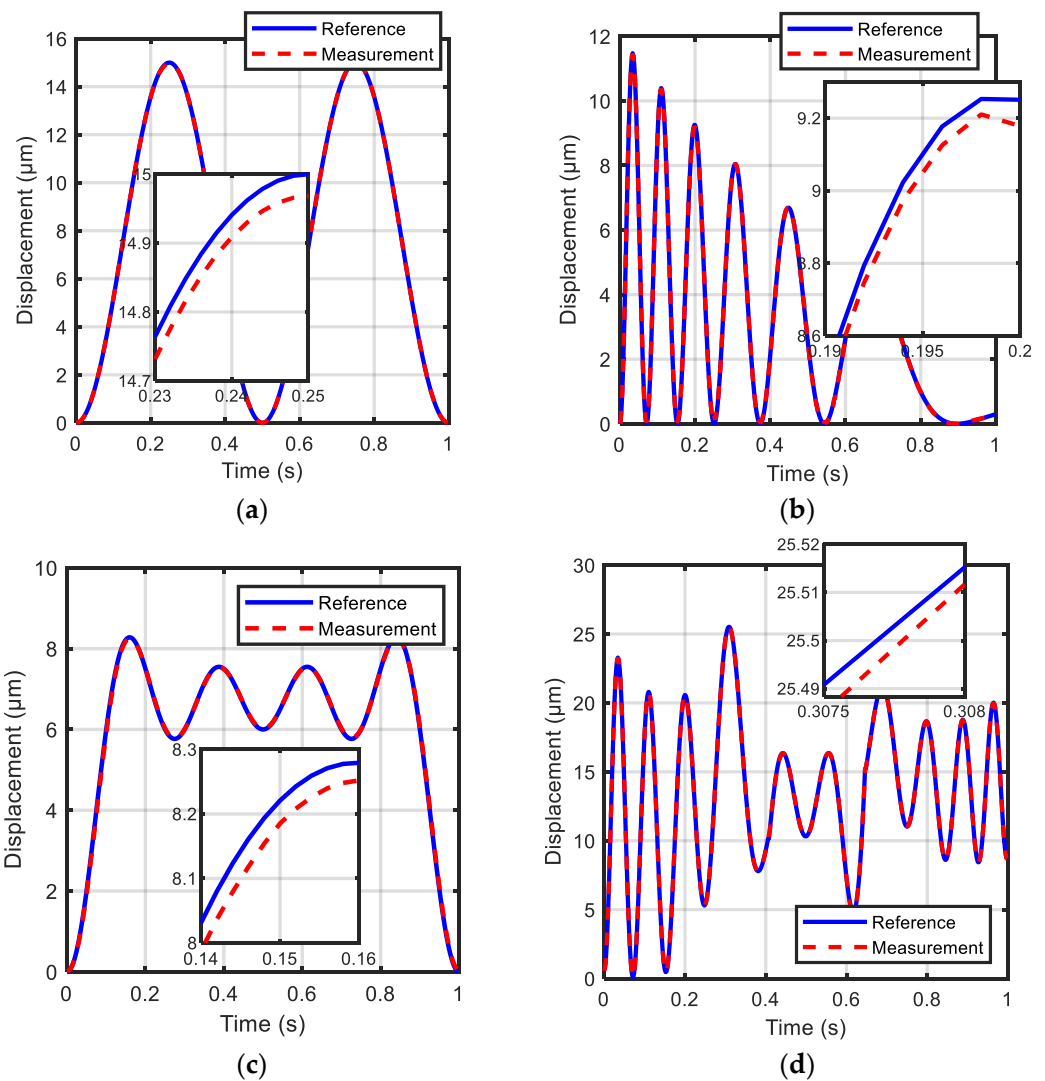


Figure 15. The laboratory results of the proposed FF control scheme: (a) test data D; (b) test data E; (c) test data F; (d) test data G. The figures show that the measured outputs track the references precisely.

4.2. Feedforward–Feedback Control and Results Comparison

To mitigate the residual errors, and hence further improve the tracking precision, the FF control was combined with FB control. This has been accomplished by summing the outputs of FF and FB controllers and then fed to the piezoelectric actuator. Figure 16 shows the block diagram of the proposed FF–FB control. The FB controller was designed

based on the incremental PID control algorithm in which the output control variable is the incremental value $\Delta u(k)$ rather than the absolute value. Thus, the control increment $\Delta u(k)$ takes the form:

$$\begin{aligned}\Delta u(k) &= u(k) - u(k-1) \\ &= K_p[e(k) - e(k-1)] + K_i e(k) + \\ &\quad K_d[e(k) - 2e(k-1) + e(k-2)]\end{aligned}\quad (22)$$

where K_p , K_i , and K_d are the proportional, integral, and derivative gains of the PID controller, respectively, and e is the displacement error. Therefore, the actuating signal of the FF–FB scheme can be expressed as:

$$\begin{aligned}v_c(k) &= v_{FF}(k) + v_{FB}(k-1) + K_p[e(k) - e(k-1)] + K_i e(k) \\ &\quad + K_d[e(k) - 2e(k-1) + e(k-2)]\end{aligned}\quad (23)$$

where v_{FF} is the output voltage of the inverse LSSVM model, and v_{FB} is the output voltage of the PID controller. From the above equation, it can be seen that there is no accumulation required and the determination of the incremental PID output is only related to the last three samplings. This makes the influence of the error action, as well as the amount of computation, relatively small. It will then be easier to obtain better results using an LSSVM-based compensator in combination with an incremental PID-based controller compared with the positional PID-based controller.

PID parameters K_p , K_i , and K_d were determined via the well-known Zeigler–Nichols formula [66] through experiments. The Zeigler–Nichols method is a heuristic method of tuning a PID controller and has been successfully used to online tune SISO stable systems. The process was carefully achieved for all trajectories in which the integral and proportional gains are initially set to zero and then the proportional gain is raised until obtaining self-sustaining oscillations that the proportional gain is called ultimate gain (K_u), and the period of sustained oscillations is called the ultimate period T_u . The optimum proportional, integral, and derivative gains are then calculated from Zeigler–Nichols tuning rules; $K_p = 0.6K_u$, $K_i = 1.2 K_u/T_u$, $0.075 K_u T_u$. A certain amount of trial and error was also used to minimize the error in the position of the signal peak. Finally, the PID parameters were fixed at $K_p = 35$, $K_i = 715$, and $K_d = 0.43$ for all test experiments.

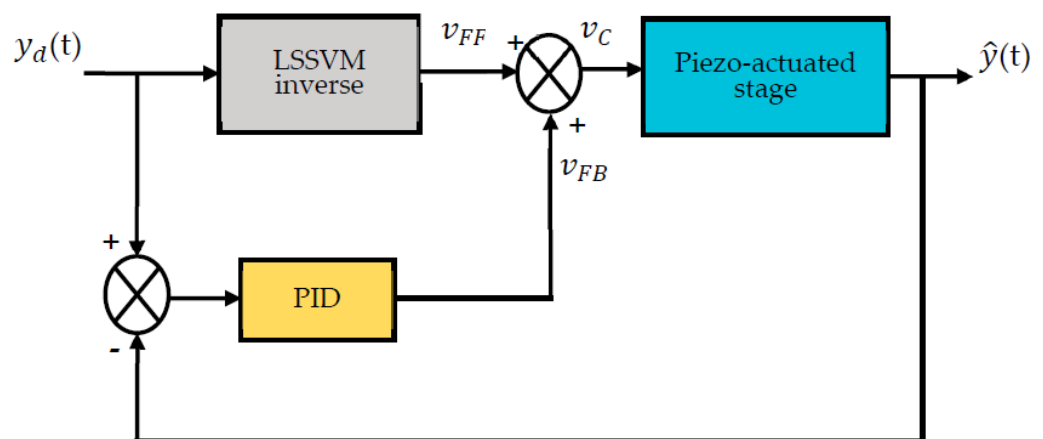


Figure 16. Block diagram of the proposed feedback–feedforward control scheme.

The datasets D, E, F, and G were also used to test the effect of the PID controller on the tracking performance. The laboratory results of the FF–FB controller for the four test samples are presented in Figure 17, it shows the measured output displacements (the output of the piezoelectric actuator) and the reference (the desired output). It produced RMSEs of 0.0214 μm , 0.0267 μm , 0.0195 μm , and 0.0250 μm , respectively, which account for 0.0611%, 0.0763%, 0.0557%, and 0.0714% of the travel range, and the mean of control results

obtained from four test datasets is $0.0232 \mu\text{m}$. It is concluded that the developed FF–FB control scheme can reduce the hysteresis nonlinearity of the piezoelectric actuator and enhance tracking capabilities better and more accurately than the proposed FF controller. The tracking results of the FF–FB control schemes have been also compared with results obtained from different FF control schemes designed using LSSVM-NARX and Preisach models, respectively, as shown in Table 7. It can be seen that the proposed FF–FB control scheme has smaller RMSE than other considered control methods and can be implemented with low execution time. Figure 18 shows the laboratory results, the error between the reference (the desired output) and the measured output displacements (the output of piezoelectric actuator), of the FF–FB control scheme and other control schemes. The results show that it has better tracking ability and its tracking errors are smaller and smoother compared with those obtained by other methods considered in our experiments.

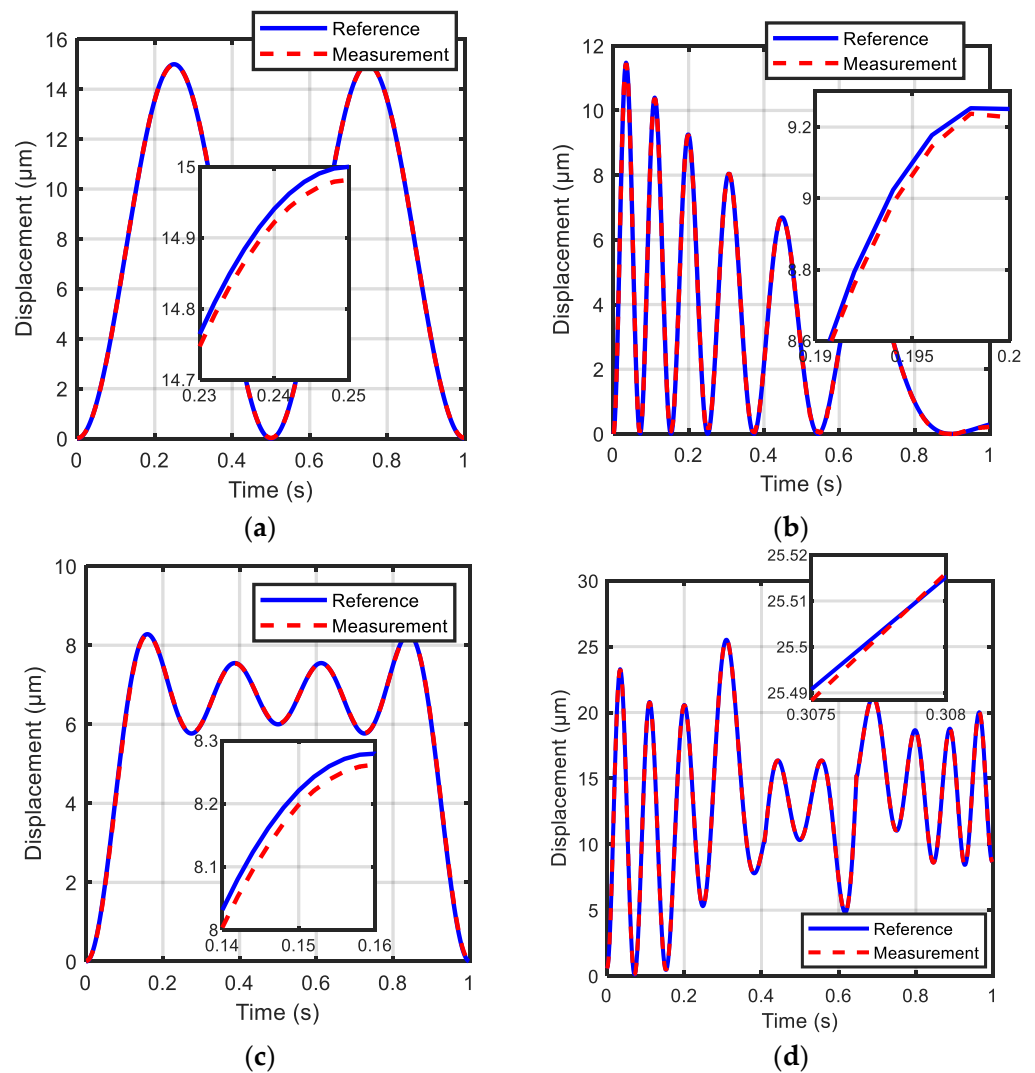


Figure 17. The laboratory results of the proposed FF–FB control scheme: (a) test data D; (b) test data E; (c) test data F; (d) test data G.

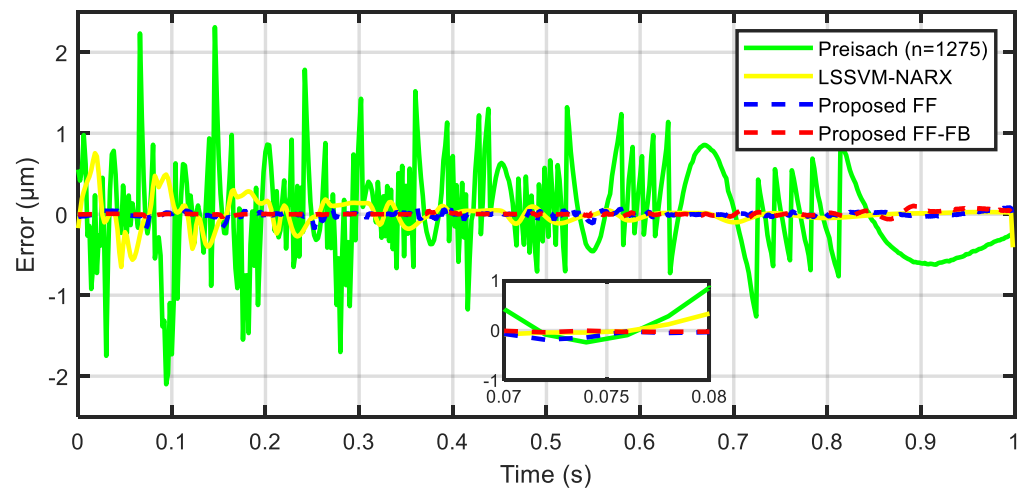


Figure 18. Tracking errors of the FF–FB control scheme compared to other control schemes on data E.

Table 7. Performance comparisons of different control schemes for dataset E.

Control Scheme	No. of Discretization Elements	RMSE (μm)	RMSE Percentage % to Travel Range	Maximum Execution Time of One Step (ms)
FF scheme with Preisach	1275	0.4981	1.4229	1.84
FF scheme with Preisach	5050	overrun	overrun	overrun
FF scheme with Preisach	7260	overrun	overrun	overrun
FF with LSSVM-NARX	-	0.1572	0.4491	0.78
The proposed FF scheme	21	0.0483	0.0683	0.55
The proposed FF scheme	28	0.0456	0.0760	0.84
The proposed FF scheme	36	0.0413	0.0883	1.21
The proposed FF scheme	55	0.0361	0.1031	1.64
The proposed FF scheme	78	overrun	overrun	overrun
The proposed FF scheme	91	overrun	overrun	overrun
The proposed FF scheme	105	overrun	overrun	overrun
The proposed FF–FB scheme	55	0.0267	0.0763	1.66

To evaluate the accuracy of our approach, we present a comparison of our results with those presented in previous studies in the area of control of piezoelectric actuators in the literature. The comparison is presented in terms of RMSEs, as in Table 8. The approach that uses LSSVM without modeling hysteresis has the highest tracking error (0.62 μm), whereas the control approach that uses the inverse LSSVM model with the NARX model for hysteresis mapping has presented better results (0.03 μm). The improved version of the classical Preisach has an RMSE of 0.15 and is better than the RNN model (0.465 μm). On the contrary, the tracking result for our proposed approach which uses an LSSVM model and hysteresis operators is superior and more accurate as its error is the best among the others (0.0232 μm). The results in this paper showed that, compared to other considered control methods and previous studies in the literature, the proposed control strategy: (1) has lower generalization errors; (2) achieves better tracking performance with a smaller number of stop operators; and (3) reduces the controller complexity compared to Preisach-based control. Therefore, we can say that the inverse PSO-LSSVM model combined with a PID feedback controller is an effective control scheme for reducing the hysteresis effects in the piezoelectric actuators.

Table 8. Comparison between the proposed method and previous studies.

Contributor	Method	RMSE
Yongcheng Xiong et al. [21]	FF control using recurrent neural networks (PEA-RNN)	0.465
Wei Tech Ang et al. [16]	FF control using the inverse of the improved Preisach (P-I) model using a linear function.	0.15
Qingsong Xu [30]	FF–FB control using LSSVM Without Modeling Hysteresis Inverse.	0.62
Liangsong Huang et al. [28]	FF–FB control using the inverse LSSVM-NARX model optimized by colony algorithm and PID controller.	0.03
The proposed method	FF–FB control using PSO-LSSVM with hysteresis operators and incremental PID controller.	0.0232

5. Conclusions

In this paper, the LSSVM model has been extended to include the case of the rate-dependent hysteresis behavior of piezoelectric actuators. The basic idea is that the learning and generalization capabilities of the proposed model are improved using a discrete memory structure and a kernel-based learning method. For this purpose, the stop hysteresis operators have been first proposed to provide a one-to-one mapping; then, the PSO-LSSVM model has been used for highly accurate training. Different datasets with a variety of hysteresis loops have been used for a more efficient evaluation of the proposed model. The simulation results demonstrated that the proposed model has significantly better generalization capability than the classical Preisach and LSSVM-NARX models. In addition, the proposed LSSVM model has a reasonable time cost due to the reduced number of stop operators required. Based on the inverse LSSVM model, two control schemes have been proposed and investigated through real-time experiments. The experimental results indicated that the combination of feedforward control and PID feedback control outperformed the feedforward control scheme in terms of tracking performance. Moreover, compared with control schemes based on the classical Preisach, which has produced RMSE of 0.498 μm and execution time of 1.84 ms, and LSSVM-NARX-based, which has produced RMSE of 0.1572 μm and execution time of 0.78, the proposed PSO-LSSVM/PID control scheme has the advantage of lower position error (RMSE = 0.0267 μm) with reasonable time complexity (execution time = 1.66).

The obtained results of this paper can be further improved with a sufficiently large numbers of hysteresis operators and training samples, and this in turn leads to higher time complexities and limits the practicability of the developed scheme. The control task also becomes more complex in the presence of cross-coupling effects in multiple axes systems. These issues should be the subject of future research.

Author Contributions: Conceptualization, A.G.B., A.S.N. and I.A.; methodology, A.G.B., A.S.N. and I.A.; software, A.G.B.; validation, A.G.B.; formal analysis, A.G.B. and A.S.N.; investigation, A.G.B., I.A. and A.A.; resources, A.G.B., I.A. and A.A.; data curation, A.G.B. and I.A.; writing—original draft preparation, A.G.B.; writing—review and editing, A.S.N. and I.A.; visualization, A.G.B. and I.A.; supervision, A.S.N. and I.A.; project administration, A.S.N., I.A. and A.A.; funding acquisition, A.S.N. and A.A. All authors have read and agreed to the published version of the manuscript.

Funding: This research received no external funding.

Institutional Review Board Statement: Not applicable.

Informed Consent Statement: Not applicable.

Data Availability Statement: All data are available in the manuscript.

Acknowledgments: This work was supported by the Researchers Supporting Project number (RSP-2021/258), King Saud University, Riyadh, Saudi Arabia.

Conflicts of Interest: The authors declare no conflict of interest.

References

1. Salapaka, S.M.; Salapaka, M.V. Scanning probe microscopy. *IEEE Control. Syst. Mag.* **2008**, *28*, 65–83.
2. Tseng, A.A.; Notargiacomo, A. Nanoscale fabrication by nonconventional approaches. *J. Nanosci. Nanotechnol.* **2005**, *5*, 683–702. [[CrossRef](#)]
3. Ewing, J.A.X. Experimental researches in magnetism. *R. Soc. Lond.* **1885**, *38*, 523–640.
4. Hassani, V.; Tjahjowidodo, T.; Do, T.N. A survey on hysteresis modeling, identification and control. *Mech. Syst. Signal Process.* **2014**, *49*, 209–233. [[CrossRef](#)]
5. Gu, G.-Y.; Zhu, L.-M.; Su, C.-Y.; Ding, H.; Fatikow, S. Modeling and control of piezo-actuated nanopositioning stages: A survey. *IEEE Trans. Autom. Sci. Eng.* **2014**, *13*, 313–332. [[CrossRef](#)]
6. Sabarianand, D.; Karthikeyan, P.; Muthuramalingam, T. A review on control strategies for compensation of hysteresis and creep on piezoelectric actuators based micro systems. *Mech. Syst. Signal Process.* **2020**, *140*, 106634. [[CrossRef](#)]
7. Al Janaideh, M.; Rakheja, S.; Su, C.-Y. Experimental characterization and modeling of rate-dependent hysteresis of a piezoceramic actuator. *Mechatronics* **2009**, *19*, 656–670. [[CrossRef](#)]
8. Naser, M.F.M.; Ikhouane, F. Characterization of the hysteresis duhem model. *IFAC Proc. Vol.* **2013**, *46*, 29–34. [[CrossRef](#)]
9. Kaltenbacher, B.; Krejčí, P. A thermodynamically consistent phenomenological model for ferroelectric and ferroelastic hysteresis. *ZAMM J. Appl. Math. Mech. Z. für Angew. Math. Und Mech.* **2016**, *96*, 874–891. [[CrossRef](#)]
10. Zhu, W.; Wang, D.-H. Non-symmetrical Bouc–Wen model for piezoelectric ceramic actuators. *Sens. Actuators A Phys.* **2012**, *181*, 51–60. [[CrossRef](#)]
11. Xiao, S.; Li, Y. Modeling and high dynamic compensating the rate-dependent hysteresis of piezoelectric actuators via a novel modified inverse Preisach model. *IEEE Trans. Control. Syst. Technol.* **2012**, *21*, 1549–1557. [[CrossRef](#)]
12. Li, Z.; Shan, J.; Gabbert, U. Inverse compensation of hysteresis using Krasnoselskii–Pokrovskii model. *IEEE ASME Trans. Mechatron.* **2018**, *23*, 966–971. [[CrossRef](#)]
13. Webb, G.V.; Lagoudas, D.C.; Kurdila, A.J. Hysteresis modeling of SMA actuators for control applications. *J. Intell. Mater. Syst. Struct.* **1998**, *9*, 432–448. [[CrossRef](#)]
14. Al Janaideh, M.; Rakheja, S.; Su, C.-Y. An analytical generalized Prandtl–Ishlinskii model inversion for hysteresis compensation in micropositioning control. *IEEE ASME Trans. Mechatron.* **2010**, *16*, 734–744. [[CrossRef](#)]
15. Mrad, R.B.; Hu, H. A model for voltage-to-displacement dynamics in piezoceramic actuators subject to dynamic-voltage excitations. *IEEE ASME Trans. Mechatron.* **2002**, *7*, 479–489. [[CrossRef](#)]
16. Ang, W.T.; Khosla, P.K.; Riviere, C.N. Feedforward controller with inverse rate-dependent model for piezoelectric actuators in trajectory-tracking applications. *IEEE ASME Trans. Mechatron.* **2007**, *12*, 134–142. [[CrossRef](#)]
17. Armin, M.; Roy, P.N.; Das, S.K. A survey on modelling and compensation for hysteresis in high speed nanopositioning of AFMs: Observation and future recommendation. *Int. J. Autom. Comput.* **2020**, *17*, 479–501. [[CrossRef](#)]
18. Delibas, B.; Arockiarajan, A.; Seemann, W. A nonlinear model of piezoelectric polycrystalline ceramics under quasi-static electromechanical loading. *J. Mater. Sci. Mater. Electron.* **2005**, *16*, 507–515. [[CrossRef](#)]
19. Serpico, C.; Visone, C. Magnetic hysteresis modeling via feed-forward neural networks. *IEEE Trans. Magn.* **1998**, *34*, 623–628. [[CrossRef](#)]
20. Ahmed, K.; Yan, P. Modeling and identification of rate dependent hysteresis in piezoelectric actuated nano-stage: A gray box neural network based approach. *IEEE Access* **2021**, *9*, 65440–65448. [[CrossRef](#)]
21. Xiong, Y.; Jia, W.; Zhang, L.; Zhao, Y.; Zheng, L. Feedforward Control of Piezoelectric Ceramic Actuators Based on PEA-RNN. *Sensors* **2022**, *22*, 5387. [[CrossRef](#)] [[PubMed](#)]
22. Khosrow-Pour, M. *Machine Learning: Concepts, Methodologies, Tools and Applications*; Information Science Reference: Hershey, PA, USA, 2012.
23. Raj, R.A.; Samikannu, R.; Yahya, A.; Mosalaosi, M. Performance evaluation of natural esters and dielectric correlation assessment using artificial neural network (ANN). *J. Adv. Dielectr.* **2020**, *10*, 2050025. [[CrossRef](#)]
24. Ukil, A. *Intelligent Systems and Signal Processing in Power Engineering*; Springer Science & Business Media: Berlin/Heidelberg, Germany, 2007.
25. Kaytez, F.; Taplamacioglu, M.C.; Çam, E.; Hardalac, F. Forecasting electricity consumption: A comparison of regression analysis, neural networks and least squares support vector machines. *Int. J. Electr. Power Energy Syst.* **2015**, *67*, 431–438. [[CrossRef](#)]
26. Haggag, S.; Nasrat, L.; Ismail, H. ANN approaches to determine the dielectric strength improvement of MgO based low density polyethylene nanocomposite. *J. Adv. Dielectr.* **2021**, *11*, 2150016. [[CrossRef](#)]
27. Suykens, J.; De Brabanter, J.; Lukas, L.; Vandewalle, J. *Least Squares Support Vector Machines*; World Scientific Publishing: Singapore, 2002.
28. Huang, L.; Hu, Y.; Zhao, Y.; Li, Y. Modeling and control of IPMC actuators based on LSSVM-NARX paradigm. *Mathematics* **2019**, *7*, 741. [[CrossRef](#)]
29. Joghataie, A.; Dizaji, M.S. Designing high-precision fast nonlinear dam neuro-modelers and comparison with finite-element analysis. *J. Eng. Mech.* **2013**, *139*, 1311–1324. [[CrossRef](#)]

30. Xu, Q. Identification and compensation of piezoelectric hysteresis without modeling hysteresis inverse. *IEEE Trans. Ind. Electron.* **2012**, *60*, 3927–3937. [CrossRef]
31. Mao, X.; Wang, Y.; Liu, X.; Guo, Y. A hybrid feedforward-feedback hysteresis compensator in piezoelectric actuators based on least-squares support vector machine. *IEEE Trans. Ind. Electron.* **2017**, *65*, 5704–5711. [CrossRef]
32. Nelles, O. *Nonlinear System Identification: From Classical Approaches to Neural Networks, Fuzzy Models, and Gaussian Processes*; Springer Nature: Berlin/Heidelberg, Germany, 2020.
33. Farrokh, M. Hysteresis simulation using least-squares support vector machine. *J. Eng. Mech.* **2018**, *144*, 04018084. [CrossRef]
34. Al Janaideh, M.; Krejčí, P. Inverse rate-dependent Prandtl–Ishlinskii model for feedforward compensation of hysteresis in a piezomicropositioning actuator. *IEEE ASME Trans. Mechatron.* **2012**, *18*, 1498–1507. [CrossRef]
35. Yusof, Y.; Mustafa, Z. A review on optimization of least squares support vector machine for time series forecasting. *Int. J. Artif. Intell. Appl.* **2016**, *7*, 35–49. [CrossRef]
36. Chebanenko, V.A.; Zhilyaev, I.V.; Soloviev, A.N.; Cherpakov, A.V.; Parinov, I.A. Numerical optimization of the piezoelectric generators. *J. Adv. Dielectr.* **2020**, *10*, 2060016. [CrossRef]
37. Eberhart, R.C.; Shi, Y.; Kennedy, J. *Swarm Intelligence*; Elsevier: Amsterdam, The Netherlands, 2001.
38. Ukil, A. Support Vector Machine. In *Intelligent Systems and Signal Processing in Power Engineering*; Springer: Berlin/Heidelberg, Germany, 2007; pp. 161–226.
39. Boser, B.E.; Guyon, I.M.; Vapnik, V.N. A training algorithm for optimal margin classifiers. In Proceedings of the Fifth Annual Workshop on Computational Learning Theory, Pittsburgh, PA, USA, 27–29 July 1992.
40. Xu, Q.; Wong, P.-K. Hysteresis modeling and compensation of a piezostage using least squares support vector machines. *Mechatronics* **2011**, *21*, 1239–1251. [CrossRef]
41. Mayergoyz, I. Mathematical models of hysteresis. *IEEE Trans. Magn.* **1986**, *22*, 603–608. [CrossRef]
42. Brokate, M.; Sprekels, J. *Hysteresis and Phase Transitions*; Springer Science & Business Media: Berlin/Heidelberg, Germany, 1996; Volume 121.
43. Farrokh, M.; Joghataie, A. Adaptive modeling of highly nonlinear hysteresis using preisach neural networks. *J. Eng. Mech.* **2014**, *140*, 06014002. [CrossRef]
44. Ascher, U.M.; Petzold, L.R. *Computer Methods for Ordinary Differential Equations and Differential-Algebraic Equations*; Siam: Philadelphia, PA, USA, 1998; Volume 61.
45. Li, B.; Tian, X. An effective PSO-LSSVM-based approach for surface roughness prediction in high-speed precision milling. *IEEE Access* **2021**, *9*, 80006–80014. [CrossRef]
46. Ren, Z.; Han, H.; Cui, X.; Qing, H.; Ye, H. Application of PSO-LSSVM and hybrid programming to fault diagnosis of refrigeration systems. *Sci. Technol. Built Environ.* **2021**, *27*, 592–607. [CrossRef]
47. De Brabanter, K.; Karsmakers, P.; Ojeda, F.; Alzate, C. *LS-SVMLab Toolbox User'S Guide: Version 1.7*; Katholieke Universiteit Leuven: Leuven, Belgium, 2010.
48. Kennedy, J.; Eberhart, R. Particle Swarms Optimization. In Proceedings of the IEEE International Conference on Neural Networks, Perth, Australia, 27 November–1 December 1995; Volume 4.
49. Physik Instrumente. P-752 High-Precision Nanopositioning Stage. Available online: <https://www.physikinstrumente.com/en/products/nanopositioning-piezo-flexure-stages/linear-piezo-flexure-stages/p-752-high-precision-nanopositioning-stage-200800/> (accessed on 14 July 2022).
50. Physik Instrumente. E-505 Piezo Amplifier Module. Available online: <https://www.physikinstrumente.com/en/products/controllers-and-drivers/nanopositioning-piezo-controllers/e-505-piezo-amplifier-module-602300/> (accessed on 15 July 2022).
51. dSPACE. DS1104 R&D Controller Board. Available online: <https://www.dspace.com/en/inc/home/products/hw/singbord/ds1104,cfm> (accessed on 14 July 2022).
52. Lai, X.; Pan, H.; Zhao, X. Adaptive control for pure-feedback nonlinear systems preceded by asymmetric hysteresis. *Energies* **2019**, *12*, 4675. [CrossRef]
53. Alturki, F.; Al-Shamma'a, A.A.; Farh, H.M.H. Simulations and dSPACE Real-Time Implementation of Photovoltaic Global Maximum Power Extraction under Partial Shading. *Sustainability* **2020**, *12*, 3652. [CrossRef]
54. Zhang, J.; Wang, X.; Shao, X. Design and real-time implementation of Takagi–Sugeno fuzzy controller for magnetic levitation ball system. *IEEE Access* **2020**, *8*, 38221–38228. [CrossRef]
55. Wiener, N. The Wiener RMS (Root Mean Square) Error Criterion in Filter Design and Prediction. In *Extrapolation, Interpolation, and Smoothing of Stationary Time Series: With Engineering Applications*; MIT Press: Cambridge, MA, USA, 1964; pp. 129–148.
56. Xavier-de-Souza, S.; Suykens, J.A.; Vandewalle, J.; Bollé, D. Coupled simulated annealing. *IEEE Trans. Syst. Man Cybern. Part B* **2009**, *40*, 320–335. [CrossRef] [PubMed]
57. Nelder, J.A.; Mead, R. A simplex method for function minimization. *Comput. J.* **1965**, *7*, 308–313. [CrossRef]
58. Stakvik, J.Å.; Ragazzon, M.R.; Eielsen, A.A.; Gravdahl, J.T. On implementation of the Preisach model identification and inversion for hysteresis compensation. *Model. Identif. Control. A Nord. Res. Bull.* **2015**, *36*, 133–142. [CrossRef]
59. Wong, P.-K.; Xu, Q.; Vong, C.-M.; Wong, H.-C. Rate-dependent hysteresis modeling and control of a piezostage using online support vector machine and relevance vector machine. *IEEE Trans. Ind. Electron.* **2011**, *59*, 1988–2001. [CrossRef]
60. Liang, X.; Qi, T.; Jin, Z.; Qian, W. Hybrid support vector machine optimization model for inversion of tunnel transient electromagnetic method. *Math. Biosci. Eng.* **2020**, *17*, 3998–4017. [CrossRef]

61. Adigüzel Mercangöz, B. *Applying Particle Swarm Optimization: New Solutions and Cases for Optimized Portfolios*; Springer: Cham, Switzerland, 2021.
62. Yamagami, T.; Jiang, J. A search for the critical slip surface in three-dimensional slope stability analysis. *Soils Found.* **1997**, *37*, 1–16. [[CrossRef](#)]
63. Tu, W.; Chen, Q. Evolution of interfacial debonding of a unidirectional graphite/polyimide composite under off-axis loading. *Eng. Fract. Mech.* **2020**, *230*, 106947. [[CrossRef](#)]
64. Chen, Q.; Wang, G. PSO-driven micromechanical identification of in-situ properties of fiber-reinforced composites. *Compos. Struct.* **2019**, *220*, 608–621. [[CrossRef](#)]
65. Aljanaideh, O.; al Janaideh, M.; Rakotondrabe, M. Inversion-free feedforward dynamic compensation of hysteresis nonlinearities in piezoelectric micro/nano-positioning actuators. In Proceedings of the 2015 IEEE International Conference on Robotics and Automation (ICRA), Seattle, WA, USA, 26–30 May 2015; IEEE: Piscataway, NJ, USA, 2015; pp. 2673–2678.
66. Ziegler, J.G.; Nichols, N.B. Optimum settings for automatic controllers. *Trans. ASME* **1942**, *64*, 759–765. [[CrossRef](#)]